Engineering Structures 362 (2026) 122874

Contents lists available at ScienceDirect

Engineering Structures

journal homepage: www.elsevier.com/locate/engstruct

Shear behavior and strength prediction model of prestressed slag-based geopolymer concrete beams

Guoxu Zhao [a], Gao Ma [a,b,*], Hyeon-Jong Hwang [c], Caijun Shi [a,**], Yunxing Du [a]

[a] College of Civil Engineering, Hunan University, Changsha 410082, China
[b] Key Laboratory for Damage Diagnosis of Engineering Structures of Hunan Province (Hunan University), Changsha, Hunan 410082, China
[c] Department of Architecture and Architectural Engineering, Seoul National University, 1 Gwanak-ro, Seoul 08826, Republic of Korea

ARTICLE INFO

Keywords:
Slag-based geopolymer concrete
Shear behavior
Prestressed beam
Shear strength model

ABSTRACT

Geopolymer concrete (GPC) has emerged as a sustainable alternative to ordinary Portland cement concrete (PCC), but its shear behavior in prestressed members remains insufficiently understood. In this study, the shear performance of 15 prestressed GPC beams was experimentally investigated and compared with that of prestressed PCC beams. Key parameters included concrete compressive strength, shear span-to-depth ratio, stirrup spacing, stirrup yield strength, and longitudinal reinforcement ratio. Test results revealed that prestressed GPC beams exhibited shear resistance comparable to that of PCC beams, but showing a 36.7%-63.3% lower diagonal cracking load, 76.1%-128.2% larger mid-span deflection at peak load, and 2.9–3.0 times wider diagonal cracks at ultimate state. The shear resistance was found to increase with higher concrete strength and longitudinal reinforcement ratio. Reducing the shear span-to-depth ratio significantly enhanced the shear resistance and accelerated the development of stirrup and tendon strains. An experimental database comprising 390 beam tests was assembled to assess the prediction accuracy of six current design codes. Comparison shows that ACI 318–25 and AASHTO 2024 provide relatively reliable predictions for prestressed beams. Based on the Rankine failure criterion and ultimate equilibrium theory, a new shear capacity model was proposed, demonstrating improved prediction accuracy for prestressed PCC and GPC beams. The findings contribute to a better understanding of the shear behavior of prestressed GPC beams and support the development of rational design methods for sustainable concrete structures.

1. Introduction

Driven by the global dual carbon targets and the increasing demand for sustainable infrastructure, the inherent drawbacks of traditional Portland cement concrete (PCC) (e.g., high carbon emissions and energy consumption) have become increasingly prominent, prompting the search for environmentally friendly and high-performance alternative materials as a key research focus in civil engineering [1,2]. Geopolymer concrete (GPC), synthesized from industrial by-products such as fly ash and slag through an alkali-activation reaction to form an inorganic polymer binder, can reduce carbon emissions by 80%-90% compared with ordinary concrete, which exhibits excellent mechanical performance, corrosion resistance, and high-temperature durability, making it a promising alternative to conventional concrete [3–5]. As critical load-resistant members in buildings and bridges, shear performance of beams directly affects structural safety and service life. The combination of prestressing techniques with geopolymer materials would provide new opportunities for lightweight and high-performance members, and the study of shear behavior in prestressed GPC beams holds significant engineering and environmental value.

Extensive research has been conducted on the shear behavior of prestressed PCC beams. Zwoyer and Siess [6] performed shear tests on prestressed concrete beams and observed that the compressive stress induced by prestressing force could effectively restrain the propagation of inclined cracks and significantly enhanced the shear capacity of beams. Elzanaty et al. [7] investigated the shear performance of prestressed beams fabricated with high-strength concrete and pointed out that although prestressing improved the mechanical state, the shear

* Corresponding author at: College of Civil Engineering, Hunan University, Changsha 410082, China.
** Corresponding author.
E-mail addresses: zhaougooxu@hnu.edu.cn (G. Zhao), magao@hnu.edu.cn (G. Ma), hwanghj@snu.ac.kr (H.-J. Hwang), cshi@hnu.edu.cn (C. Shi), duyunxing@hnu.edu.cn (Y. Du).

https://doi.org/10.1016/j.engstruct.2026.122874
Received 24 January 2026; Received in revised form 13 April 2026; Accepted 30 April 2026

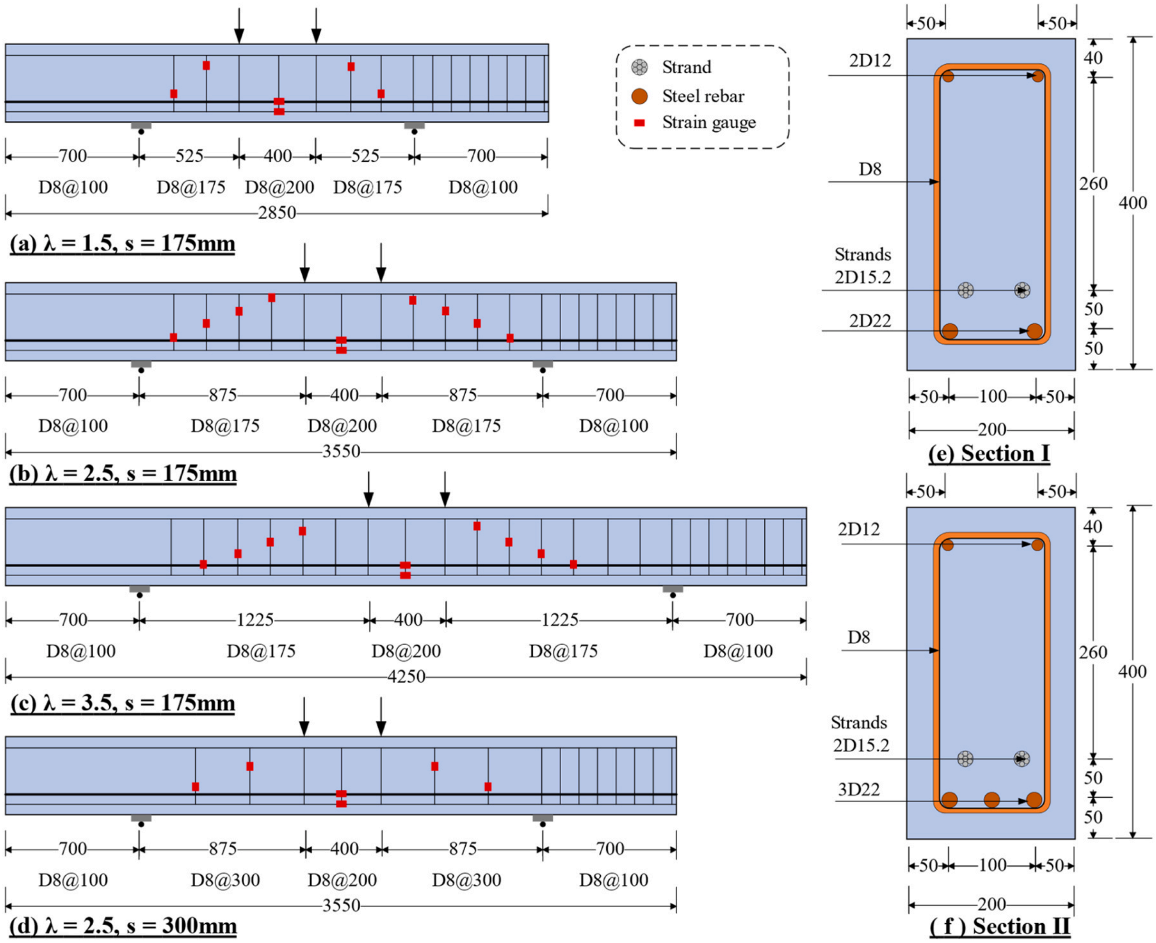

Fig. 1. Configuration and reinforcement details of specimens (unit: mm).

strength increased with the increase of prestressing force; Rupf et al. [8] carried out tests on post-tensioned I-shaped beams and found that the prestress level affected the sectional stress distribution and governed the shear strength and failure mode of prestressed concrete beams in combination with the amount of shear reinforcement and presence of flanges. Park et al. [9] verified a strain-based shear strength model and demonstrated that prestressing force significantly improved the shear capacity of PC beams by adjusting the compression zone depth and cracking moment, with a more pronounced enhancement for beams with large shear span ratios.

Existing studies on the shear behavior of GPC beams are focus mainly on non-prestressed members [10–15], and there are very few investigations that specifically focus on the shear behavior of prestressed GPC beams, with most relevant publications [16–20] taking prestressed GPC beams as the research object but not prioritizing shear performance. This has severely restricted the popularization and application of GPC. Existing studies reported that non-prestressed GPC beams exhibited certain shear behavior characteristics similar to those of PCC beams. Both materials exhibited similar crack development patterns under shear force, such as the development of diagonal cracks and shear strength contributions of aggregate interlocking and dowel action [21, 22]. However, due to intrinsic differences in microstructure and interface properties, their shear mechanisms exhibited distinct features. Consequently, GPC beams showed greater brittleness, faster crack propagation, and lower shear ductility compared with PCC beams with the same concrete strength [15,23]. Zhang et al. [24] conducted static tests on ten reinforced concrete (RC) beams and found that textile-reinforced geopolymer mortar (TRGM) increased shear resistance by 47%-106%, though the cracking load was lower than that of beams strengthened with ordinary mortar. Wu et al. [25] investigated 18 slag-based GPC beams under shear and observed that while shear resistance and failure modes were comparable to those of ordinary concrete beams, the cracking load was lower. Shear span-to-depth ratio (a/d) had a significant effect on the normalized shear strength, and the concrete strength contributed to the shear strength as a function of $(f_c')^{0.65}$. Madheswaran et al. [26] reported that for thin-web T-beams, shear span-to-depth ratio (1.9 and 2.5) and stirrup spacing significantly influenced shear performance, and predictions of ACI 318–08 [27] were conservative but suitable for preliminary design. Aldemir et al. [28] produced GPC beams using construction and demolition waste (CDW) and found comparable shear performance to ordinary concrete beams. Irmawaty et al. [29] demonstrated that in precast GPC mortar panel retrofitting, use of anchor bolts and mesh reinforcement could enhance shear capacity by 14.1%-34.9% and improve the ductility. GPC members are prone to cracking. The application of prestress can increase the cracking load of GPC members and promote their engineering application.

Despite these advances, available systematic research on prestressed GPC beams remains limited: (1) Most studies focus on non-prestressed GPC beams [24–26,28,29], leaving the coupling effect of prestressing and geopolymer material properties on the shear mechanisms unclear, and systematic data on crack development and reinforcement strain distribution under prestressing force are lacking; (2) Quantitative influence of key design parameters, such as shear span-to-depth ratio, longitudinal reinforcement ratio, stirrup configuration (spacing and strength), on the shear performance of prestressed GPC beams is not fully established, and comparative analyses with PCC are scarce [22,25]; (3) Existing shear strength prediction models, such as GB50010–2010

Table 1
Parameters of test specimens.

Specimens	Length (mm)	Shear span (mm)	a/d	f_{co} (MPa)	f_t (MPa)	f_{ps0} (MPa)	A_s (mm^2)	ρ_s (%)	s (mm)
C50-λ2.5-N175-I	3550	875	2.5	50.62	3.42	1214.5	760.3	0.29	175
C70-λ2.5-N175-I	3550	875	2.5	70.47	4.10	1214.5	760.3	0.29	175
G50-λ1.5-N175-I	2850	525	1.5	47.31	3.29	1214.5	760.3	0.29	175
G50-λ2.5-N175-I	3550	875	2.5	47.31	3.29	1129.7	760.3	0.29	175
G50-λ3.5-N175-I	4250	1225	3.5	47.31	3.29	1129.7	760.3	0.29	175
G50-λ2.5-N300-I	3550	875	2.5	47.31	3.29	1129.7	760.3	0.17	300
G50-λ2.5-H175-I	3550	875	2.5	47.31	3.29	1201.5	760.3	0.29	175
G50-λ2.5-H300-I	3550	875	2.5	47.31	3.29	1138.9	760.3	0.17	300
G50-λ2.5-H175-II	3550	875	2.5	47.31	3.29	1201.5	1140.4	0.29	175
G70-λ1.5-N175-I	2850	525	1.5	66.99	3.99	1216.4	760.3	0.29	175
G70-λ2.5-N175-I	3550	875	2.5	66.99	3.99	1216.4	760.3	0.29	175
G70-λ3.5-N175-I	4250	1225	3.5	66.99	3.99	1216.4	760.3	0.29	175
G70-λ2.5-H175-I	3550	875	2.5	66.99	3.99	1201.5	760.3	0.29	175
G70-λ2.5-H300-I	3550	875	2.5	66.99	3.99	1138.9	760.3	0.17	300
G70-λ2.5-H300-II	3550	875	2.5	66.99	3.99	1138.9	1140.4	0.17	300

Note: l is the total length of tested specimen. a and d are the shear span and depth of the beam, respectively. f_{co} is the cubic concrete compressive strength and f_t is the concrete tensile strength. f_{ps0} is the effective prestressing stress obtained from load sensor before tendon release. A_s is the cross-sectional area of longitudinal reinforcement. ρ_s and s are the stirrups ratio and spacing, respectively.

[30], ACI 318–25 [31], and AASHTO 2024 [32], are based on ordinary concrete tests; Wu et al. [25] noted that current design codes underestimated shear strength of slag-based GPC beams, and Visintin et al. [22] reported that MC2010 [33] showed deviations up to 33% for GPC beams without stirrups, while the applicability of current design codes to prestressed GPC beams has not yet been evaluated; and (4) Theoretical models remain non-specific, as most GPC shear models are adopted from ordinary concrete models [24,28] without fully accounting for prestressing effect and geopolymer properties, and no equilibrium-based formulas at the ultimate state have been established for these members. Choi et al. [34,35] proposed a method for beam shear capacity based on Rankine criterion [36]. However, this approach did not account for the influence of prestressing force. Subsequently, Park and Choi [9] further developed the model to incorporate prestressing factors. While this model demonstrated high accuracy in predicting shear resistance, it required an iterative process to calculate the compression zone depth and concrete strain. Further, use of a layered discretization method makes it less practical for engineering applications.

Based on the above research gaps, this study focuses on the shear performance of prestressed GPC beams through systematic experimental and theoretical analyses. Beam shear tests were performed to investigate the load-deflection behavior, crack evolution, and reinforcement strain distribution, comparing the performance of GPC and PCC beams. The effects of shear span-to-depth ratio, longitudinal reinforcement ratio, stirrup ratio, and stirrup strength on the shear performance were quantitatively evaluated. Current design codes including GB50010–2010 [30], ACI 318–25 [31], AASHTO 2024 [32], CEB-FIP 2010 [33], Eurocode 2 [37], and JGC 15 [38] were applied to the test results, and the prediction accuracy was systematically compared. The Rankine criterion, as an important branch of ultimate equilibrium theory, has been widely applied in strength analysis of geotechnical and concrete structures [39] and provides a reliable theoretical basis for deriving shear capacity for prestressed GPC beams [40]. For this reason, shear capacity model for prestressed GPC beams was proposed based on the Rankine criterion and ultimate equilibrium methods, providing experimental evidence and theoretical support for their engineering design and application.

2. Test program

2.1. Test specimens

Fig. 1 illustrates the configuration and reinforcement details of the shear test specimens, including 15 specimens with different parameters (Fig. 1(a)-(d)) and two rectangular cross-section types (Fig. 1(e)-(f)). The test parameters are the concrete type (PCC or GPC), concrete strength (50 or 70 MPa), shear span-to-depth ratio ($\lambda = 1.5$, 2.5, or 3.5), stirrup spacing ($s = 175$ or 300 mm), longitudinal reinforcement ratio (0.95 or 1.43%), and stirrup strength (350 or 420 MPa). For section I, 2-D12 deformed bars were used for compression bars, and 2-D15.2 prestressing tendons and 2-D22 deformed bars were used for tension bars. In section II, 2-D22 deformed bars in tension were replaced with 3-D22 deformed bars. All specimens were designed to exhibit shear failure. For sufficient anchorage of strand at the beam ends, D8 bars were used for stirrups at a spacing of 100 mm over the 700 mm end regions [30,31]. Detailed specimen information is presented in Table 1.

The specimen naming convention combines series symbols with parameter designations. The initial letter "C" represents PCC, while "G" denotes GPC, followed by a number indicating the concrete strength grade. The subsequent "λ" and number indicate the shear span-to-depth ratio (e.g., "λ2.5" corresponds to a shear span-to-depth ratio of 2.5). The letter following the shear span-to-depth ratio, "N" or "H", denotes the stirrup strength, with "N" for normal-strength ($f_y = 350$ MPa) stirrups and "H" for high-strength ($f_y = 420$ MPa) stirrups. The number after the stirrup designation indicates stirrup spacing in millimeters. Roman numerals at the end, such as "I" or "II", indicate the cross-section type. For example, specimen C50-λ2.5-N175-I represents an ordinary concrete beam with a C50 strength grade, shear span-to-depth ratio of 2.5, normal-strength stirrups at a spacing of 175 mm, and cross-section type I.

2.2. Material properties

The mix proportions of the PCC and GPC beams are listed in Table 2. The preparation of GPC involves three main components: binder,

Table 2
Mix proportion of PCC and GPC (kg/m3).

Concrete	Cement	Slag	Fly ash	Silica fume	Sand	Gravel	Na_2CO_3	Sodium silicate solution	NaOH	Super-plasticizer	Water
PCC50	457	-	114	-	696	1044	-	-	-	4.57	160
PCC70	450	120	-	20	610	1070	-	-	-	15	138
GPC50	-	350	116	-	674	1055	12	163.2	12.3	-	83.3
GPC70	-	397	100	-	661	1034	17	214.2	15.2	-	38.8

Table 3
Chemical compositions of slag and fly ash (wt%).

	SiO_2	Al_2O_3	CaO	MgO	K_2O	Fe_2O_3	Na_2O	SO_3
Slag	33.81	14.78	38.81	7.09	0.44	0.36	0.26	2.49
Fly ash	54.22	31.18	1.24	0.47	1.34	2.36	0.49	0.35

Table 4
Concrete strength development with age.

	7d (MPa)	14d (MPa)	28d (MPa)
PCC50	31.78	40.20	50.62
PCC70	56.72	61.83	70.47
GPC50	39.08	43.94	47.31
GPC70	58.67	63.14	66.99

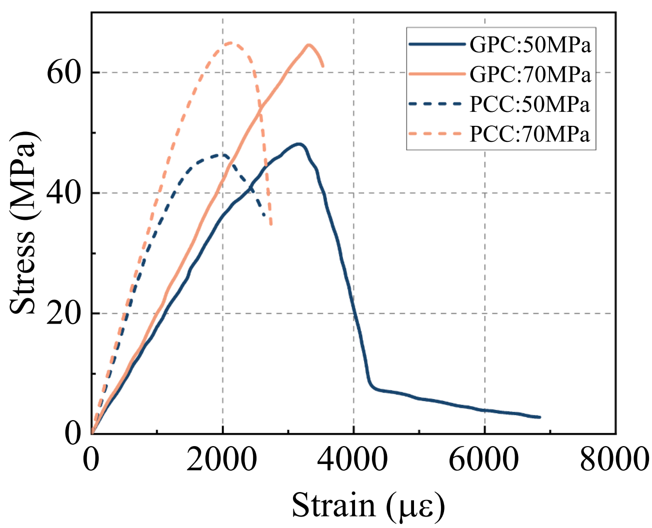

Fig. 2. Stress-strain curve of GPC.

alkaline activator, and aggregates. The binder consisted of fly ash being Class F and slag with a density of 2880 kg/m^3 and a specific surface area of 426 m^2/kg. Table 3 shows the chemical composition of the slag and fly ash. For PCC, C50 and C70 concrete were prepared with P.O 42.5 R cement and P.O 52.5 R cement, respectively. The alkaline activator comprised waterglass and sodium hydroxide. The waterglass had the chemical formula $Na_2O{\cdot}nSiO_2$ with a modulus of n = 3.31 and a water content of 64.8%. Prior to casting, the activator solution was prepared in advance, sealed, and cooled to room temperature to prevent carbonation and moisture loss. For aggregates, crushed stone with a particle size range of 5–20 mm and a density of 1623 kg/m^3 was used as coarse aggregate, while fine aggregate had the maximum particle size of 4.51 mm and a density of 1466 kg/m^3 .

Table 5
Mechanical properties of steel bars and tendons.

Steel bars and tendons	Diameter (mm)	f_y (MPa)	f_u (MPa)
HPB300	8	350	396.2
HRB400	8	420	546.2
HRB400	22	420	540.3
Strand-15.2	15.2	1860.5	1922.7

The preparation procedure for slag-based GPC is as follows: first, the pre-weighed sand, sodium carbonate, fly ash, and slag were added to a mixer. The prepared alkaline activator and water were then added while the mixer was running. Coarse aggregate was subsequently added, and mixing continued until a homogeneous concrete mixture was achieved. The fresh geopolymer concrete paste was immediately cast into molds and compacted using a needle-type vibrator to prevent excessive air bubbles and surface honeycombing.

Concrete strength was tested at 7, 14 and 28 days after concrete casting. Table 4 shows the concrete strength development under indoor curing conditions of approximately 30°C. Once the concrete specimens reached 75% of their specified strength, prestressing tendons were released. Concrete cubes were cured under the same conditions as the beams. According to GB/T 50081–2019 [41], the compressive strength f_{cu} of concrete was measured on testing day using 150 mm × 150 mm × 150 mm standard cubes (Fig. 3(a)). The stress–strain curves of GPC and PCC obtained from 100 mm × 100 mm × 300 mm prismatic specimens are compared in Fig. 2. The concrete strength of different specimens can be seen in Table 1. Based on the extensive previous experimental data [25,42,43] on geopolymer concrete the axial compressive strength ($f_c = \alpha_{c1} f_{co}$) and axial tensile strength (f_t=0.395 $(f_{co})^{0.55}$) can be calculated in accordance with GB/T 50152–2012 [44], where α_{c1} is 0.76 and 0.79 for concrete with strengths of 50 MPa and 70 MPa, respectively. The elastic modulus of concrete was measured using prismatic specimens of 100 mm× 100 mm× 300 mm (Fig. 3(b)), and calculated from $E_c = (F_a - F_0)L/A\Delta n$, where F_a is 1/3 of the axial compressive strength; F_0 is the initial load corresponding to concrete compressive stress of 0.5 MPa; A is the cross-sectional area of the concrete specimen; L is the measurement length of dial gauge; and Δn is the average deformation on both sides. The elastic modulus of 50 MPa and 70 MPa PCC was 32.39 GPa and 34.71 GPa, respectively, whereas the corresponding value for GPC was 24.19 GPa and 28.62 GPa. The properties of reinforcements and tendons were prepared and tested in

(a) Compressive strength test of concrete (b) Elastic modulus test of concrete (c) Tensile strength test of rebar

Fig. 3. Test of the mechanical properties of materials.

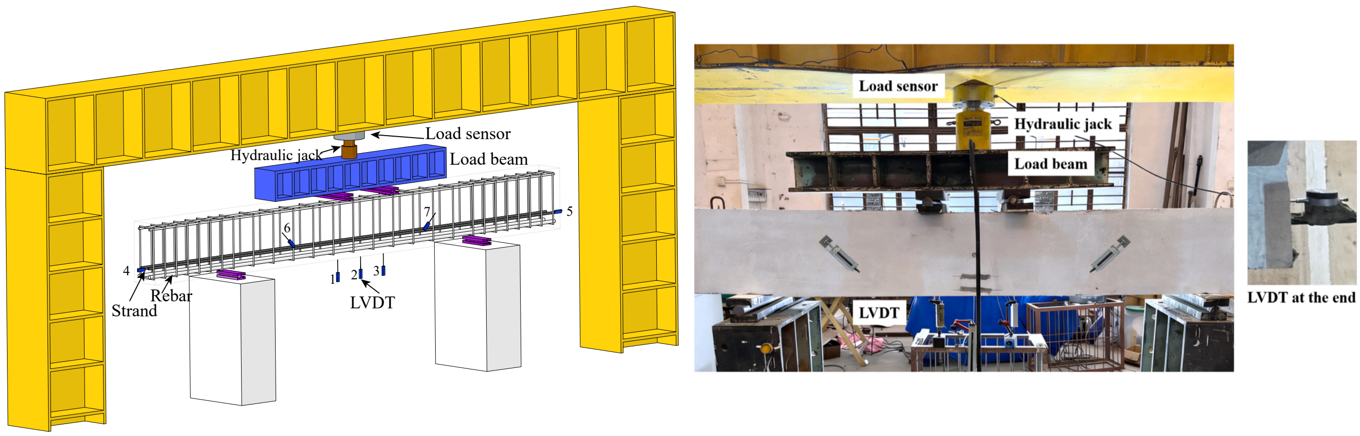

Fig. 4. Test setup.

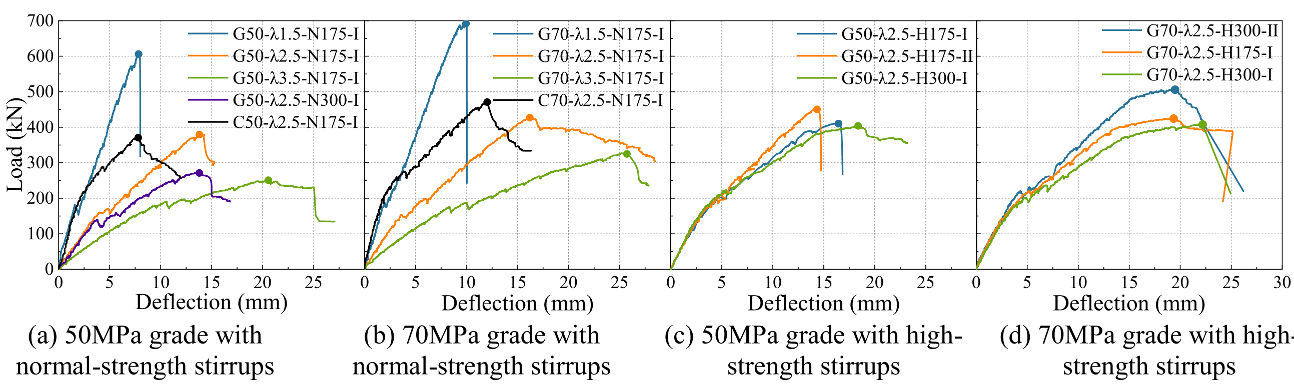

(a) 50MPa grade with normal-strength stirrups (b) 70MPa grade with normal-strength stirrups (c) 50MPa grade with high-strength stirrups (d) 70MPa grade with high-strength stirrups

Fig. 5. Load-deflection relationship of test specimens.

accordance with standard test methods for metallic materials, with gauge lengths appropriately set for reinforcing bars and steel strands, respectively. All tensile tests were carried out on a universal testing machine (Fig. 3(c)) in accordance with GB/T 28900 [45] for reinforcing steel and GB/T 21839 [46] for steel strands, and no fewer than three specimens were tested for each material to ensure repeatability. The properties of steel bars and tendons can be seen in Table 5.

2.3. Test setup and instrumentation

As shown in Fig. 4, four-point loading was applied at the mid-span of the beam specimens. The load was applied manually using a hydraulic jack, and a 1000 kN load cell was employed to measure the applied load. Prior to the development of flexural cracks, the load increased in increments of 5 kN. Once flexural cracks appeared, subsequent load increments were set at 10% of the theoretical shear resistance P_u. After the onset of diagonal shear cracks, the load increased in increments of 5% of P_u until specimen failure.

A total of seven linear variable differential transformers (LVDTs) were installed on each beam to measure deflections at mid-span and loading points (LVDT 1–3), as well as potential slip of the prestressing tendons at both ends (i.e., LVDT 4 and 5 were installed to the exposed end of the prestressing tendons). Two additional LVDT 6 and 7 were arranged along a line perpendicular to the line connecting the loading points and supports to monitor the development of diagonal shear cracks. Strain gauges (marked in red in Fig. 1) were installed on the stirrups in shear span region and the prestressing tendons in constant-moment region to capture the strain response during loading. DIC acquisition system was also used to collect the strain on the surface of the specimen. During each loading increment, the deflection, load at

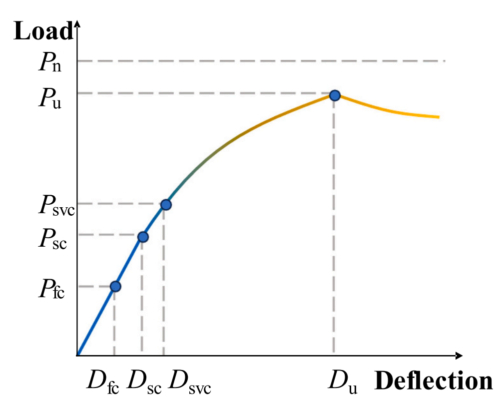

Fig. 6. typical load-deflection curve of prestressed concrete beams under shear loading.

first flexural crack, diagonal crack formation, and subsequent crack propagation were recorded.

3. Test results

3.1. Load-deflection relationship

Fig. 5 presents the load-deflection curves of multiple groups of test beams. Due to the characteristics of four-point bending test, half of the peak load corresponds approximately to the shear strength of beam specimens. The curves show that before the development of diagonal cracks, the specimens remain largely in a linear-elastic state, after which

Table 6
Test results of test specimens.

Specimens	P_{fc} (kN)	D_{fc} (mm)	P_{sc} (kN)	D_{sc} (mm)	P_u (kN)	D_u (mm)	P_n (kN)	P_u/P_n	P_{svc} (kN)	P_{svc}/P_u	s_u (mm)	Failure mode
C50-λ2.5-N175-I	136.5	1.30	313.5	5.50	370.5	7.8	508.6	0.73	315.9	0.85	0	S
C70-λ2.5-N175-I	154.0	1.27	270.0	4.1	470.8	12.0	568.1	0.83	272.6	0.58	0	S
G50-λ1.5-N175-I	126.0	1.05	155.0	2.0	606.2	7.8	827.7	0.73	160.0	0.26	0.37	S
G50-λ2.5-N175-I	57.0	1.36	170.0	4.1	379.3	13.9	496.6	0.76	190.8	0.50	0.22	S
G50-λ3.5-N175-I	30.0	1.17	190.0	10.8	250.8	20.6	354.7	0.71	191.3	0.76	0.29	FS
G50-λ2.5-N300-I	52.0	1.38	125.0	3.8	271.4	13.5	496.6	0.55	223.1	0.82	0.38	S
G50-λ2.5-H175-I	102.0	1.94	190.0	4.5	413.8	16.8	496.6	0.83	195.9	0.47	0.31	S
G50-λ2.5-H300-I	80.0	1.43	188.0	4.7	403.9	18.4	496.6	0.81	199.3	0.49	0.43	FS
G50-λ2.5-H175-II	72.9	1.32	189.5	4.2	450.4	14.3	595.2	0.76	295.7	0.66	0.33	S
G70-λ1.5-N175-I	75.0	0.78	180.0	1.7	693.2	9.9	935.0	0.74	180.3	0.26	0.30	S
G70-λ2.5-N175-I	70.0	1.11	154.0	4.1	427.0	16.3	561.0	0.76	154.5	0.36	0.29	S
G70-λ3.5-N175-I	35.0	1.20	175.0	8.4	327.0	25.2	400.7	0.82	187.5	0.57	0.59	S
G70-λ2.5-H175-I	92.0	1.52	220.0	5.3	425.8	19.2	561.0	0.76	223.2	0.52	0.58	F
G70-λ2.5-H300-I	81.0	1.46	191.2	4.5	407.8	22.1	561.0	0.73	200.7	0.49	0.39	S
G70-λ2.5-H300-II	65.6	1.00	220.0	4.08	507.20	19.5	656.2	0.77	220.3	0.43	0.5	F

Note: P_{fc} and D_{fc} are the flexural cracking load and corresponding mid-span deflection, respectively; P_{sc} and D_{sc} are the diagonal cracking load and corresponding mid-span deflection, respectively; P_u and D_u are the peak load and corresponding mid-span deflection, respectively; P_n and P_{svc} is the nominal flexural load and service load, respectively; s_u is the slip length of strand end at the ultimate state; S represents shear failure; and FS represents flexure-shear failure; F represents flexural failure. The graphical meaning of all characteristic load/deflection notations is illustrated in Fig. 6 with a typical load-deflection curve of prestressed concrete beams under shear loading.

internal forces are redistributed. The stiffness of the specimens is primarily governed by the propagation of diagonal cracks rather than flexural cracks, and once diagonal cracks develop within the shear span, beam deflection increases sharply.

Prestressed GPC specimens exhibited the peak loads comparable to those of ordinary PCC (with a 2.8% lower shear capacity for 50 MPa GPC and 5.6% higher for 70 MPa PCC), while the specimens with a compressive strength of $f_{co} \approx 70$ MPa achieved 43.4% higher peak loads noticeably higher peak loads than the specimens with $f_{co} \approx 50$ MPa, indicating that increasing concrete strength enhanced the load-carrying capacity. A lower shear span-to-depth ratio of 1.5 increased the peak load compared with larger shear span-to-depth ratios of 2.5 or 3.5, with the shear capacity of GPC beams decreasing by 37.4%-38.4% (λ=2.5) and 52.8%-58.6% (λ=3.5), suggesting that an increase in shear span-to-depth ratio reduced the shear resistance. Regarding stirrup parameters, specimens with normal-strength stirrups (N) at a spacing of 175 mm achieved higher peak loads than those with 300 mm spacing, and specimens with high-strength stirrups (H) outperformed the specimens with normal-strength stirrup at the same spacing, indicating that reducing stirrup spacing and increasing stirrup strength improved the load resistance. Differences in cross-sectional configuration also affected structural performance, with specimens having higher longitudinal reinforcement ratios (Section II) exhibiting slightly higher (11.0%) ultimate loads than Section I specimens, confirming that the beneficial effect in shear strength of longitudinal reinforcement cannot be neglected. Furthermore, peak deflection and post-peak ductility varied with parameters: specimens with larger shear span-to-depth ratios and wider stirrup spacing displayed more pronounced post-peak deflection, high-strength 70 MPa GPC specimens exhibited more gradual post-peak stiffness degradation, whereas PCC specimens showed more brittle behavior following shear failure.

3.2. Crack patterns and failure modes

Fig. 7 illustrates the failure modes of 15 beam specimens and the surface strain results measured by DIC at the ultimate state. As shown in Fig. 7(a), failure types can be mainly classified into three categories: flexural failure, flexure-shear failure, and shear failure. Flexural failure occurred in specimens G70-λ2.5-H175-I and G70-λ2.5-H300-II. This exceptional outcome may be attributed to the inherent variability of the concrete or subjective factors during specimen preparation and testing. Flexure-shear failure occurred in specimens G50-λ3.5-N175-I and G50-λ2.5-H300-I, in which severe diagonal cracking developed before crushing of the top concrete, leading to excessive yielding of stirrups. The failure types of the test specimens (i.e., shear failure, flexure-shear failure, and flexural failure) were rigorously classified by combining direct observation of the ultimate failure state and quantitative analysis of the load-deflection curves. The failure modes of all beams are summarized in Table 6.

The development of cracks can be divided into three stages: Stage 1: Initially, vertical flexural cracks develop at mid-span, gradually propagating toward the supports and evolving into diagonal cracks, forming diagonal crack paths from the support to the loading point. Stage 2: When diagonal cracks propagate from the support toward the loading point, the process occurs suddenly, accompanied by a "pop" sound, and a notable jump in load occurs, resulting in a clear inflection point in the load-deflection curve. At this stage, some slip of the prestressing strands can be detected at the cracked end. Stage 3: As the load continues to increase, cracks around the diagonal cracks propagate and eventually penetrate the entire web cross-section, leading to sudden brittle failure accompanied by a loud fracture sound, with a rapid strength degradation.

Fig. 7(b) shows the distribution of the maximum principal strain on the specimen surfaces. It can be observed that the strain-concentrated regions correspond to the shear failure planes within the shear span. The strain contours exhibit a typical diagonal band pattern, reflecting the propagation path of diagonal cracks during shear tests. It is evident that the crack development in PCC and GPC is generally similar. For GPC, higher longitudinal reinforcement ratio decreased the spacing and width of cracks. Specimens with high-strength stirrups exhibited wider and more numerous flexure-shear cracks compared to the counterparts with normal-strength stirrups, due to the increased shear capacity and deformation capacity imparted by the high-strength stirrups. In contrast, specimens with low stirrup ratios (e.g., G50-λ2.5-N300-I) demonstrated lower load resistance, and flexural cracks were less pronounced.

Fig. 8 compares the development of the maximum width of the main diagonal crack width, measured between LVDT 4 and 5, in accordance with load. Crack widths were automatically measured using LVDTs (refer to Fig. 4). As shown in Fig. 8(a) and (b), under identical shear span-to-depth ratios (λ2.5) and stirrup spacings, the diagonal crack widths (0.51–1.60 mm) at ultimate load in PCC beams were smaller than 1.49–4.60 mm in GPC beams (about 3.0 times wider for GPC), and the diagonal cracking load (270.0–313.5 kN) of PCC specimens was higher than 154.0–170.0 kN of GPC specimens G50-λ2.5-N175-I and G70-λ2.5-N175-I (36.7%–63.3% lower for GPC). This phenomenon is attributed to the more brittle behavior of GPC compared with PCC. In addition, an

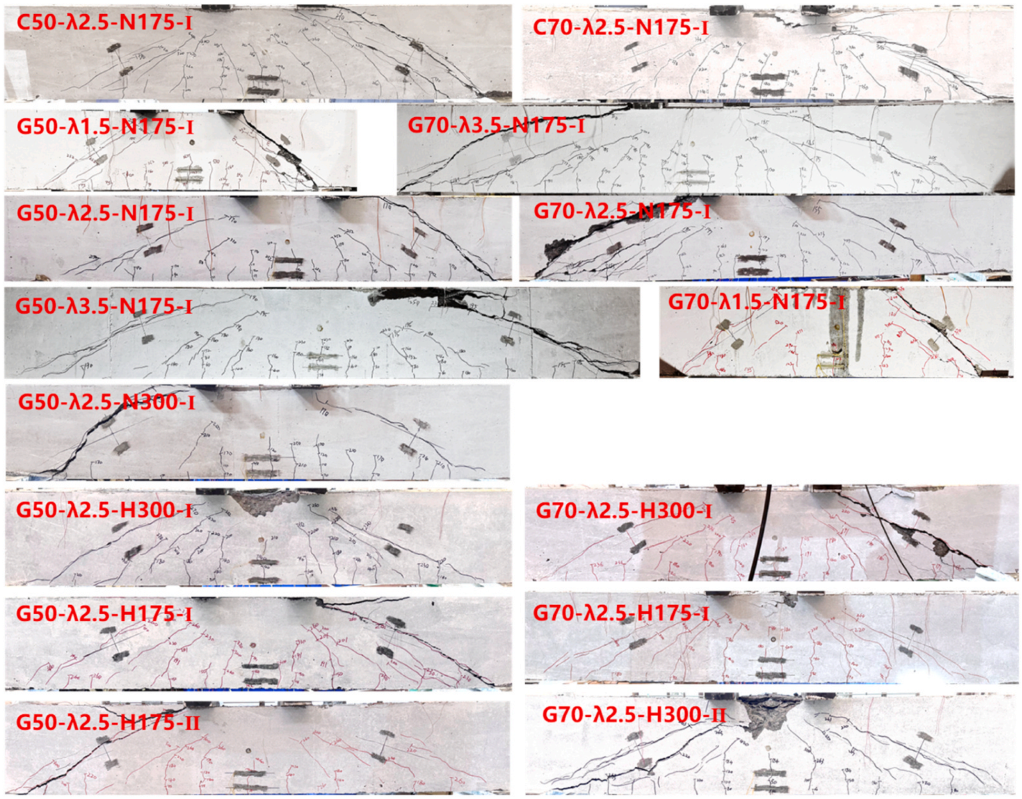

(a) Crack pattern and failure mode

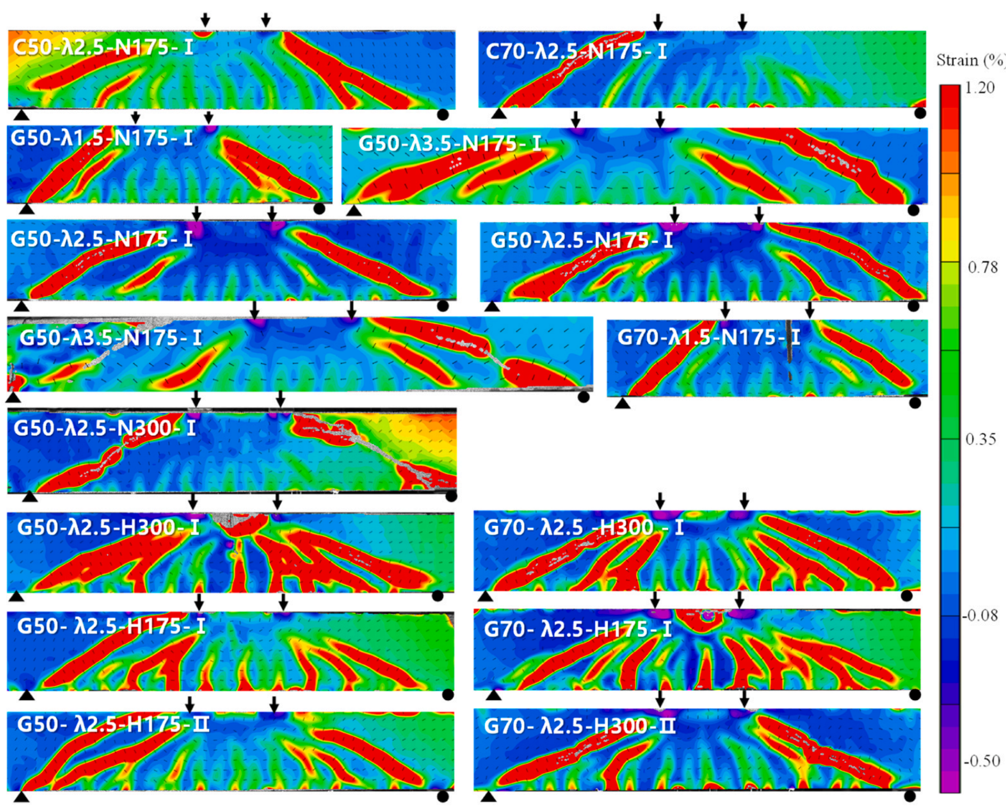

(b) DIC results at failure state (max principal strain)

Fig. 7. Crack pattern and failure mode and DIC results.

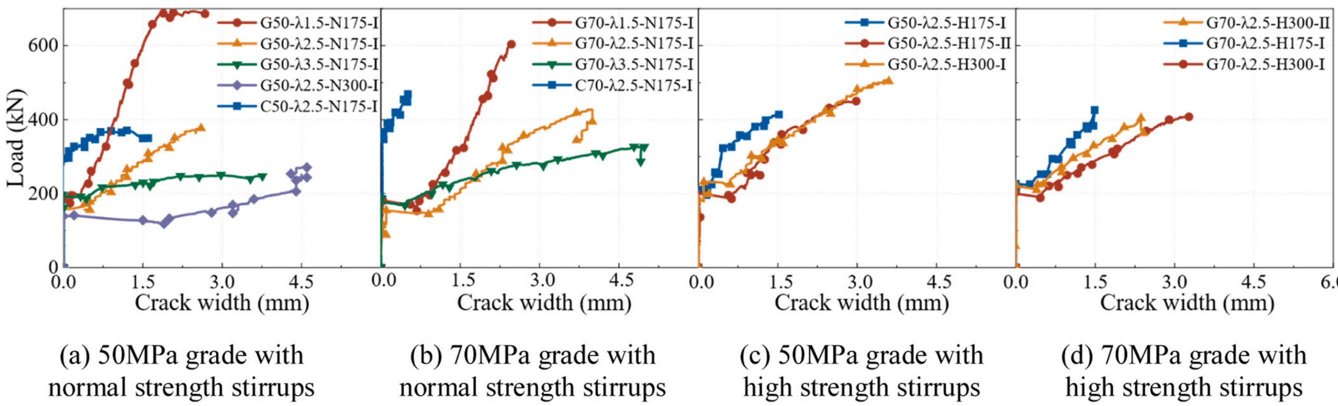

Fig. 8. Crack versus load curves.

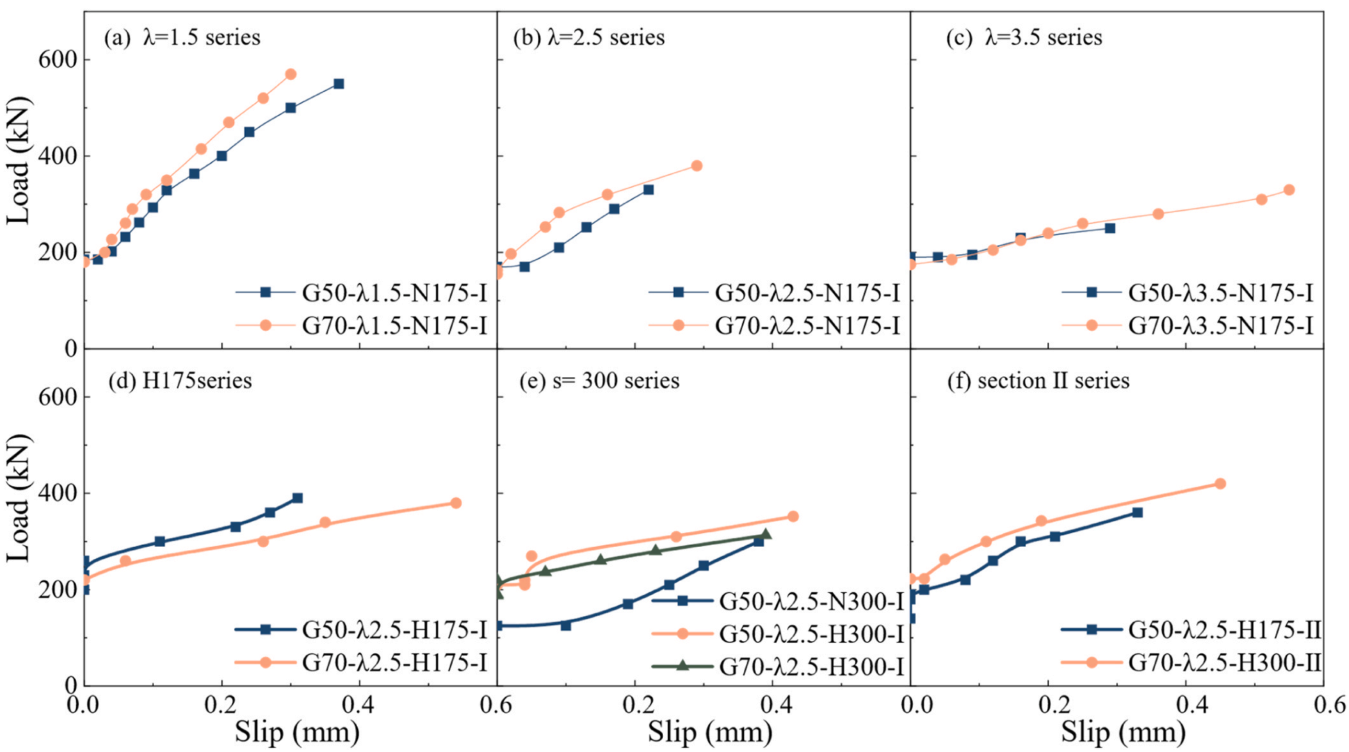

Fig. 9. Load versus strand slip response.

increase in shear span-to-depth ratio leads to larger crack widths. Due to the increased stirrup spacing, the diagonal crack width of specimen G50-λ2.5-N300-I increased rapidly once diagonal cracking initiated. The use of high-strength stirrups effectively restrains rapid crack widening, while increasing the longitudinal reinforcement ratio can also suppress crack width development to a certain extent.

According to GB 50010–2010 [30], the allowable maximum crack width under normal indoor environmental conditions is 0.30 mm, while a limit of 0.20 mm is specified for aggressive environments. For this reason, the service load (V_{svc}) was taken as the load corresponding to a crack width of 0.2 mm. Both the diagonal cracking strength and V_{svc} were determined based on LVDT measurements. At the early loading stage, flexural cracks first appeared; with increasing load, diagonal cracks formed, whose widths were initially smaller than flexural crack widths. Beyond a certain load level, the diagonal crack width exceeded the flexural crack width and became dominant. A lower ratio of service load to ultimate shear strength (V_{svc}/V_u) indicates a higher reserve strength. The average V_{svc}/V_u ratio of GPC beams was approximately 0.49(with a 31.9% lower strength reserve ratio than PCC beams), whereas that of PCC beams was about 0.72. In addition, the values of

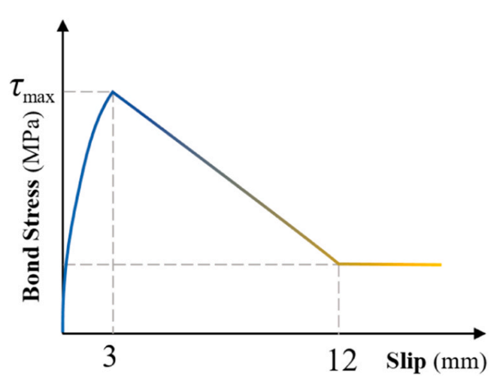

Fig. 10. Bond-slip relationship between strand and concrete [47].

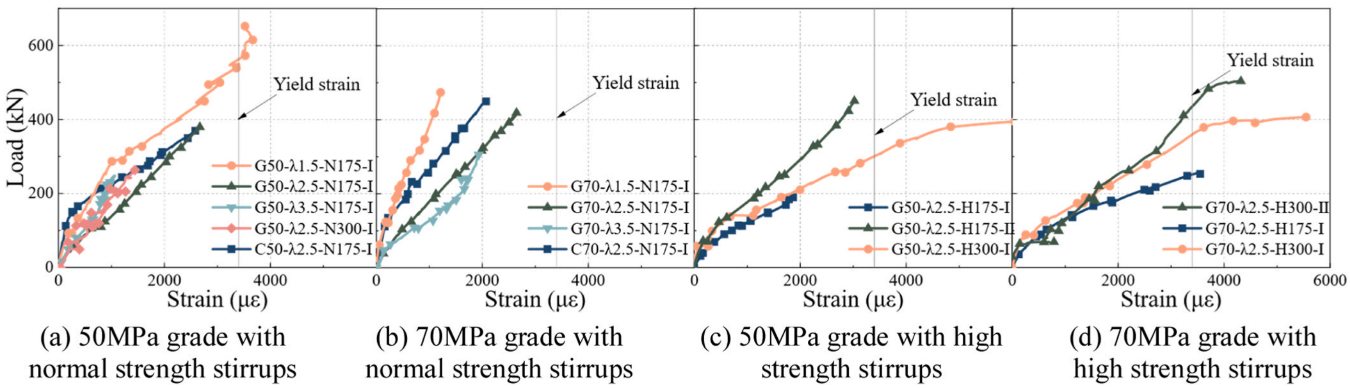

Fig. 11. Strain of pretensioned tendon.

diagonal cracking load (P_{sc}) and service load (P_{svc}) were very close, indicating that the serviceability limit state occurred shortly after the development of diagonal cracks.

Fig. 9 compares the relationship between tendon slip and applied load. During the tests, a certain amount of end slip of the prestressing tendons was observed in all GPC specimens. The onset of tendon slips consistently coincided with the development of diagonal cracks. When the bond-slip of strand is less than 3 mm, it can be considered that no bond failure occurs (Fig. 10) [47]. As seen in Fig. 9, the measured slip values were less than 0.6 mm, indicating that bond failure of the prestressing tendons did not occur and that the end anchorage length satisfied design code requirements. Concrete strength and shear span-to-depth ratio had a pronounced influence on tendon slip. Higher concrete strength provided greater bond strength to the prestressing tendons, thereby reducing slip. In contrast, a larger shear span-to-depth ratio resulted in a greater bending moment under the same vertical load, which increased the tension force transmitted to the tendons and generated larger slip. By comparison, stirrup spacing and longitudinal reinforcement ratio exhibited no noticeable influence on tendon slip.

3.3. Strain of reinforcement

Fig. 11 compares the development of prestressing tendon strain for prestressed GPC and PCC beams under shear loading. Due to premature failure of strain gauges, the reinforcement strain data for specimens G50-λ3.5-N175-I and G50-λ2.5-N300-I were incomplete. Under identical shear span-to-depth ratios and stirrup configurations, GPC beams generally exhibited comparable or slightly higher prestressing tendon strain levels than PCC beams. This behavior can be attributed to the lower elastic modulus of GPC beams [48,49], which results in reduction in deformation stiffness and thus larger flexural deformation under the same load. The shear span-to-depth ratio λ had a pronounced influence on tendon strain development: compared with specimens with $\lambda = 3.5$, those with $\lambda = 1.5$ and 2.5 showed a slower increase in tendon strain under the same load. With increasing shear span-to-depth ratio, the beams tended to exhibit more pronounced flexural behavior, resulting in higher tensile strain of prestressing tendons. Note that except for the specimens governed by flexure-shear failure and flexural failure, the tendon strains at failure in all other specimens were generally less than or equal to the yield strain. Specimens reinforced with high-strength stirrups or with smaller stirrup spacing exhibited more pronounced tendon strain growth, indicating that stronger or high stirrups ratio effectively restrained diagonal crack propagation and enhanced shear resistance, thereby increasing overall flexural deformation of the beam. A comparison between section I and section II specimens with identical parameters showed that beams with higher longitudinal reinforcement ratios (section II) generally exhibited lower tendon strains at the same load level and a significantly higher load corresponding to tendon yielding. This result demonstrates that an increased longitudinal reinforcement ratio enlarges the compression zone depth, which in turn enhances the overall stiffness and delays tendon yielding, thereby improving the shear performance of

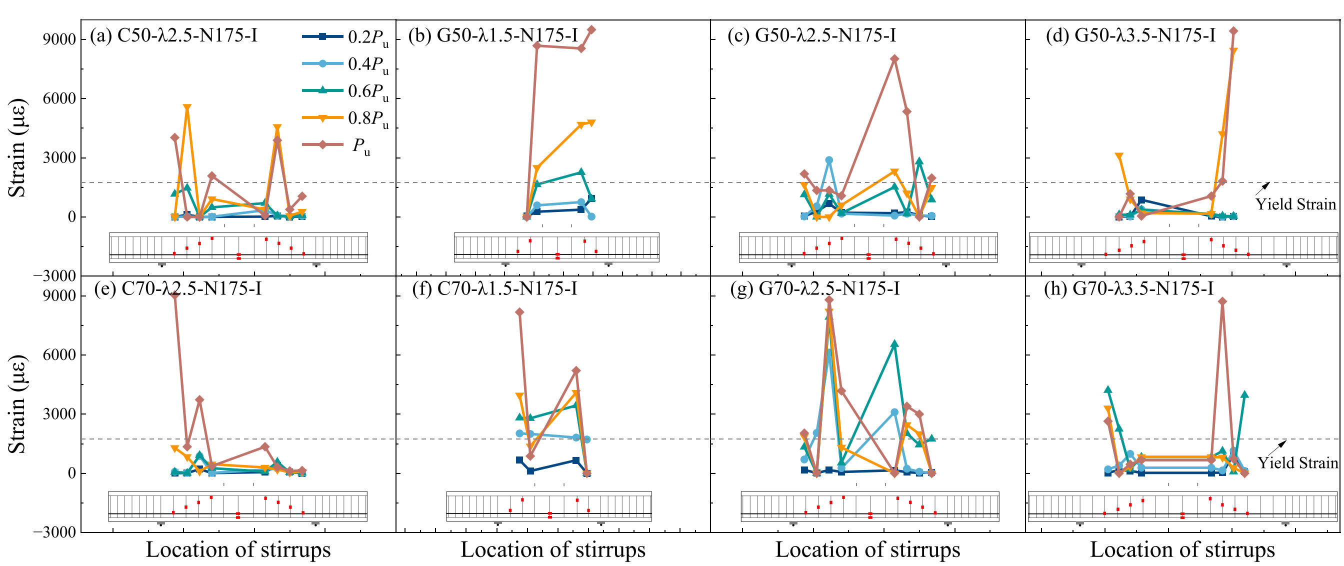

Fig. 12. Strain of stirrups in different specimens.

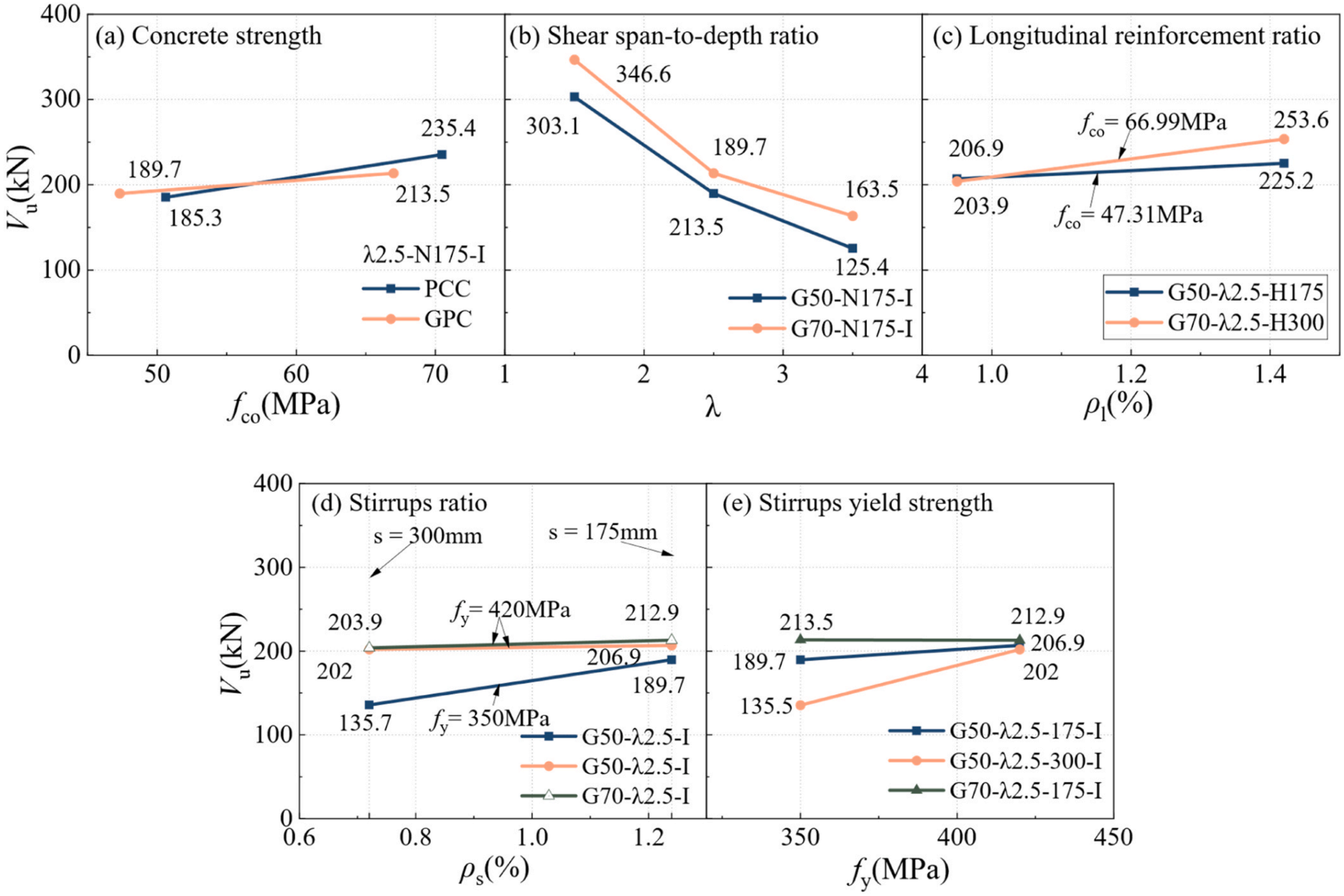

Fig. 13. Effect of test parameters on shear strength.

prestressed GPC beams.

Fig. 12 compares the distribution of stirrup strain along the beam length at representative loading stages (0.2 P_u, 0.4 P_u, 0.6 P_u, 0.8 P_u, and peak load P_u) in beam specimens. The dashed line denotes the stirrup yield strain and is used to evaluate the stress state of the stirrups and their level of participation during shear failure process. At low load levels (0.2 P_u and 0.4 P_u), stirrup strains in all specimens remained relatively small, indicating that shear resistance was mainly provided by the concrete diagonal compression struts, while the stirrups were not yet significantly engaged. As the load increased to 0.6P_u and 0.8 P_u, stirrup strains within the shear span increased markedly and gradually concentrated toward the support, reflecting the initiation and propagation of diagonal cracks and the progressive activation of stirrups in restraining crack development.

Near the peak load P_u, most specimens exhibited localized surges in stirrup strain within the shear span, with some measurement points exceeding the yield strain, indicating a transition of the shear-resisting mechanism from "concrete-dominated" to a combined action of concrete and stirrups. Except for specimen C70-λ2.5-N175-I where stirrup yielded only on one side, all other specimens showed stirrup yielding on both sides of the loading point. This symmetry in yielding is attributed to the extensive development of severe diagonal cracks on both sides. It should be noted that the strain readings are highly dependent on the relative position of the strain gauges to the diagonal cracks; a significant strain increase is typically observed only when a major diagonal crack passes directly through or very near the gauge location. Compared with beams having $\lambda = 3.5$, beams with smaller shear span-to-depth ratios ($\lambda = 1.5$ and 2.5) more pronounced stirrup strain development at both ends and were more prone to stirrup yielding at P_u. This behavior is attributed to the dominance of shear effects at small shear span-to-depth ratios, where diagonal cracks develop earlier and propagate rapidly and concrete strut resists a larger portion of shear force directly to the supports. Under identical shear span-to-depth ratios and stirrup configurations, GPC and PCC beams showed similar stirrup strain distribution patterns, both characterized by evident strain concentration within the shear span. Increasing the concrete strength from 50 MPa to 70 MPa reduced stirrup strains below 0.6P_u load levels, and the load at which stirrups yielded increased from 0.8 P_u to P_u, suggesting that higher-strength concrete effectively delayed diagonal crack development and thereby reduced the load demand on stirrups. However, this phenomenon was less pronounced in GPC beams. For the GPC specimens, the diagonal cracking loads were relatively low, ranging between 125 kN and 190 kN, and showed no significant variation. As observed in Fig. 12, widespread stirrup yielding did not occur in all specimens at P_u; in most cases, yielding was limited to a few stirrups near the main diagonal crack, indicating that shear failure of prestressed concrete beams was still primarily governed by concrete crushing of diagonal strut or instability of diagonal cracking.

4. Discussion of test results

4.1. Effect of slag-based geopolymer concrete

Fig. 13 compares the influence of test parameters on the shear capacity of prestressed concrete beams. As shown in Fig. 13(a), the shear capacities of GPC beams were comparable to those of PCC beams. Compared with the GPC beams, the shear capacity of the 50 MPa PCC beam was approximately 2.8% lower (i.e., 189.7 kN for GPC beam and 185.3 kN for PCC beam), whereas for the 70 MPa grade, the PCC beam exhibited a 5.6% higher shear capacity than the GPC beam (i.e., 213.5 kN for GPC beam and 235.4 kN for PCC beam). However, Fig. 7 indicates that under the same load level, GPC beams exhibit significantly larger mid-span deflections than PCC beams. For specimens C50-λ2.5-N175-I and C70-λ2.5-N175-I, the mid-span deflections were 7.9 mm and 12.3 mm at P_u, respectively, whereas the corresponding values increased to 13.9 mm and 17.7 mm at P_u for specimens G50-λ2.5-N175-I and G70-λ2.5-N175-I. Similar observations were reported in previous study [25]. This is because elastic modulus of GPC was approximately 20–30% lower than that of PCC. As discussed earlier, both the flexural cracking load and diagonal cracking load of GPC beams were lower than those of PCC specimens, and the crack widths in GPC beams were generally larger. This is mainly because slag-based GPC exhibits poorer crack resistance compared with PCC. For this reason, the ratio of strength reservation (P_{svc}/P_u) in PCC beams (0.58–0.85) was higher than that in GPC specimens (0.26–0.82).

The above analysis further elucidates the systematic behavioral discrepancies between GPC and PCC beams. While the compressive strength of GPC governs its ultimate shear capacity, the intrinsically distinct tensile properties, elastic modulus, and interfacial bond behavior of GPC control the early-stage cracking, deflection, and crack propagation. This also confirms that the shear design method for PCC beams, which focuses on compressive strength, may capture the ultimate shear capacity of GPC beams, but cannot accurately predict their serviceability performance.

4.2. Effect of shear span-to-depth ratio

As shown in Fig. 13(b), shear span-to-depth ratio λ had a pronounced influence on the shear capacity of prestressed concrete beams. For both 50 MPa and 70 MPa concrete grades, a consistent trend was observed with increasing λ. When the λ increased from 1.5 to 2.5 and 3.5, the shear capacities of the 50 MPa beams decreased by 37.4% and 58.6%, respectively, while those of the 70 MPa beams decreased by 38.4% and 52.8%. Although the shear capacity decreased significantly with the increase of λ, the diagonal cracking loads of the specimens showed no substantial variation. As summarized in Table 3, the diagonal cracking loads of G50 specimens with λ ranging from 1.5 to 3.5 remain within 170–190 kN, whereas those of G70 specimens were 155–180 kN. This is because the initiation and development of diagonal cracks are governed primarily by the concrete strength to shear resistance. The contribution of stirrups to the shear capacity becomes effective only after the development of diagonal cracks. For the specimens with low λ, the dominant arch action means that the ultimate shear capacity is almost entirely determined by the compressive resistance of the diagonal concrete strut, which is the core reason for the similar ultimate shear strength between GPC and PCC beams.

4.3. Effect of longitudinal reinforcement ratio

As seen in Fig. 13(c), increasing the longitudinal reinforcement ratio also enhanced the shear capacity of prestressed concrete beams, which was consistent with the findings reported in the literature [25]. However, except ACI 318–25 [31] and JGC-15 [38], other codes don't explicitly consider the contribution of flexural reinforcement to shear capacity. For G50 concrete beams with longitudinal reinforcement ratios of 0.95% and 1.42%, the corresponding shear capacities are 203.9 kN and 225. 2 kN, respectively, representing an increase of approximately 11.0% in shear strength. Similarly, even though specimen G70-λ2.5-H300-II failed in flexure, its ultimate load capacity was still 25.0% higher than that of G70-λ2.5-H300-I. This result indicates that the influence of longitudinal reinforcement ratio on the shear strength cannot be neglected. For the section II specimens (G50-λ2.5-H175-II and G70-λ2.5-H300-II), the P_{svc} was 295.7 kN and 220.3 kN, respectively. In contrast, the corresponding specimens with lower reinforcement ratios (G50-λ2.5-H175-I and G70-λ2.5-H300-I) exhibited P_{svc} of 195.9 kN and 200.7 kN, respectively. These results demonstrate that an increased longitudinal reinforcement ratio significantly improves the crack resistance of prestressed concrete beams and contributes positively to their shear performance.

Table 7
Existing shear strength models for prestressed and non-prestressed concrete beams.

Investigator	Shear strength models
GB50010-2010 [30][1]	$V_n = V_{cs} + V_{pGB}$
	$V_{cs} = \alpha_{cv} f_t b_w d + f_v \frac{A_{sv}}{s} d$
	$V_{pGB} = 0.05 N_{p0}$
ACI 318-25 [31][2]	$V_n = V_c + V_s$
	V_c should be less of
	$V_{ci} = 0.05\lambda_l \sqrt{f_c'} b_w d + V_d + \frac{V_i M_{cre}}{M_{max}} \geqslant 0.14\lambda_l \sqrt{f_c'} b_w d$ and $V_{cw} = (0.29\lambda\sqrt{f_c'} + 0.3 f_{pc}) b_w d + V_p$,
	$V_s = A_v f_v d/s$
AASHTO-2024 [32][3]	$V_n = V_c + V_s + V_p$
	$V_c = 0.0316\beta\sqrt{f'_c} b_w d$
	$V_s = A f_v d_v (\cot\theta + \cot\alpha)\sin\alpha / s$
CEB-FIP Model Code 2010 [33][4]	$V_n = V_c + V_s \leqslant k_c \frac{f_{ck}}{\gamma_c} b_w z \frac{\cot\theta + \cot\alpha}{1 + \cot^2\theta}$
	$V_c = k_v \frac{\sqrt{f_{ck}}}{\gamma_c} z b_w$
	$V_s = A_v z f_v (\cot\theta + \cot\alpha)\sin\alpha / s$
EuroCode 2 [37][5]	$V_n = V_c + V_s$
	$V_c = [0.12k(100\rho_p f_c')^{1/3} + \sigma_{cp}] b_w d \geqslant [0.035 k^{3/2}\sqrt{f_c'} + 0.15\sigma_{cp}] b_w d$
	$V_s = A_v d f_v \cot\theta / s \leqslant b_w d_v f_{cd} / (\cot\theta + \tan\theta)$
JGC-15 [38][6]	$V_n = V_c + V_s + V_{ped}$
	$V_c = \beta_d \cdot \beta_p \cdot \beta_n \cdot f_{vcd} \cdot b_w \cdot d / \gamma_b$
	$V_s = \left(A_v f_v (\sin\alpha_s + \cos\alpha_s)/s + A_{pv}\sigma_{pv}(\sin\alpha_p + \cos\alpha_p)/s_p\right)/\gamma_b$

Note: [1] α_{cv} is a coefficient related to the shear span-to-depth ratio; defined as $1.5 \le \alpha_{cv} = 1.75/(\lambda + 1) \le 3$; and N_{p0} denotes the effective prestressing force on the concrete section when the tensile stress at the concrete edge is zero; f_y is the yield strength of stirrups.
[2] V_s is the shear force provided by stirrups; λ_l is the lightweight concrete coefficient (= 1.0 in this study); The cracking moment is calculated as $M_{cre} = (I/y_t)(0.5\lambda\sqrt{f'_c} + f_{pe} - f_d)$; I is the moment of inertia of the section, and y_t is the distance from the centroid to the extreme tensile fiber; V_{ci} is the flexure-shear strength; and V_{cw} is the web-shear strength; V_p is the component in the direction of the applied shear of the effective prestressing force.
[3] θ and α is angle of inclination of diagonal compressive stresses and angle of inclination of transverse reinforcement to longitudinal axis.
[4] $k_c = 0.5(30/f_{ck})^{1/3} \le 0.55$; z is internal lever arm; f_{ck} characteristic value of cylinder compressive strength of concrete; and γ_c partial safety factor for concrete material properties (= 1.0 for direct comparison in this study).
[5] $k = 1 + \sqrt{200/d} \le 2.0$; $\rho_p \leqslant 0.02$; $\sigma_{cp} = P_e/A_c < 0.2 f_{cd}$; and A_c is the gross sectional area of beam; f_c' and f_{ctd} are the design values of concrete compressive and tensile strengths, respectively.
[6] V_{ped} is the vertical component of effective prestress force; $f_{vcd} = 0.20\sqrt[3]{f'_{cd}}$; f'_{cd} is the design compressive strength of concrete; $\beta_d = \sqrt[4]{1000/d}$;; $p_v = A_s/(b_w d)$; A_s area of tension reinforcement;; M_o decompression moment necessary to cancel stress due to axial force at extreme tension fiber; M_{ud} is the design flexural moment capacity; and γ_b is the safety factor (= 1.3 in general and 1.0 for direct comparison in this study).

4.4. Effect of stirrups ratio and stirrups yield strength

As shown in Fig. 13(d), an increase in ρ_s increased the shear capacity for both G50 and G70 specimens. For instance, in the G50-λ2.5 series, increasing the stirrup ratio from approximately 0.7% to 1.2% resulted in an increase in V_u from 135.7 kN to 189.7 kN, corresponding to an improvement of nearly 40%. Note that because specimen G70-λ2.5-H175-I failed in flexure, increasing the stirrup reinforcement ratio had a limited effect on enhancing its ultimate load capacity compared with G70-λ2.5-H300-I. At lower ρ_s, the shear resistance was dominated by the

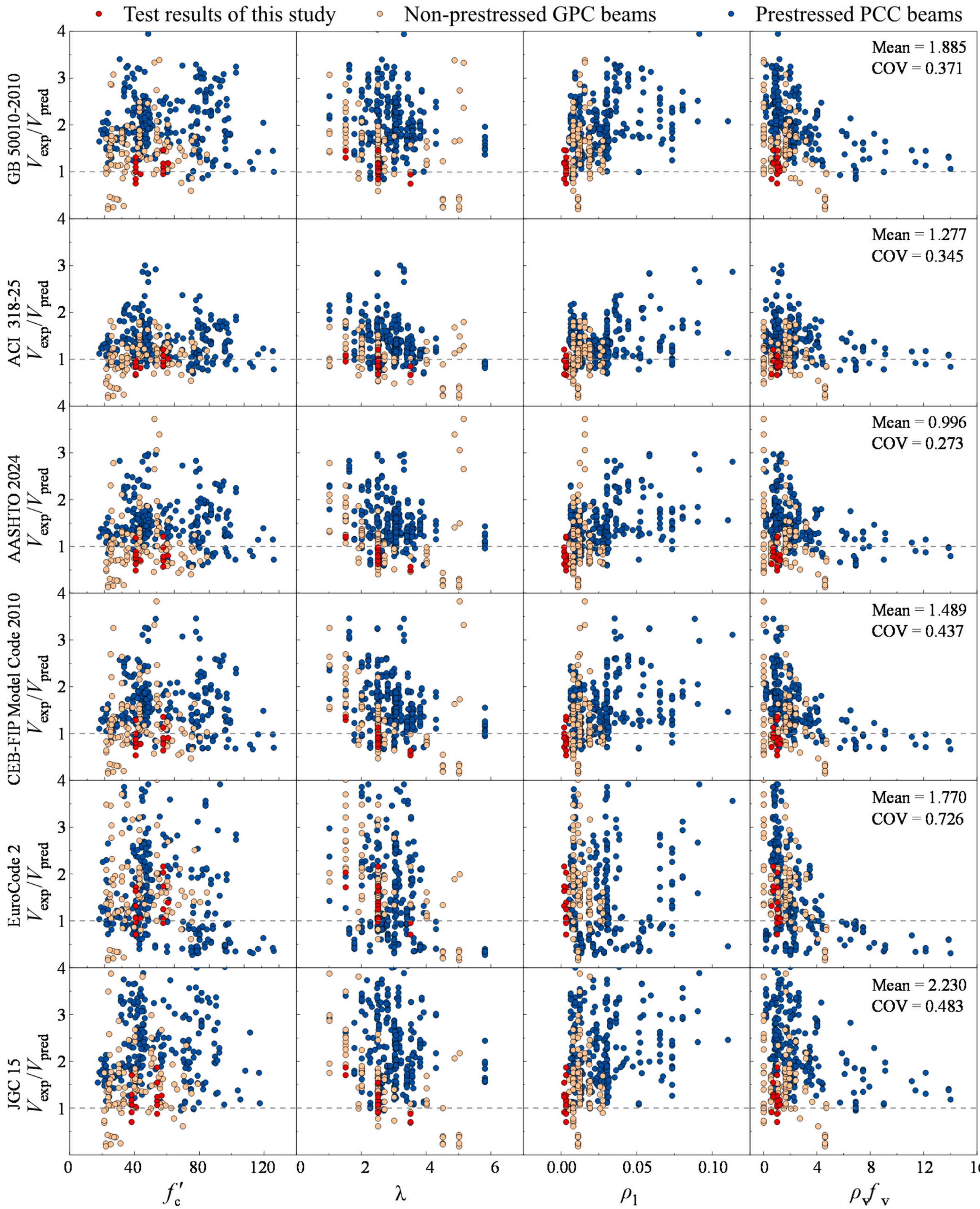

Fig. 14. Comparison of test results with predictions of current design codes.

concrete contribution, whereas with increasing ρ_s, the stirrup contribution became increasingly significant for beams reinforced with normal-strength stirrups.

The effect of stirrup yield strength on the shear capacity is presented in Fig. 13(e), comparing specimens reinforced with normal-strength (f_y = 350 MPa) stirrups and high-strength (f_y = 420 MPa) stirrups, while maintaining comparable stirrup ratios and spacing. This result indicates that increasing the stirrup yield strength leads to a moderate but consistent increase in V_u. In G50-λ2.5 series with stirrup spacing of 175 mm, increasing f_y from 350 MPa to 420 MPa improved the shear capacity from approximately 189.7 kN to 206.9 kN (i.e., an increase of about 9.1%). However, for the corresponding G50-λ2.5 series with a stirrup spacing of 300 mm, the shear capacity increased from 135.7 kN to 202.0 kN (i.e., an increase of about 49.0%). A comparable trend is not observed in G70 series, because for high-strength concrete, the spacing of 175 mm is already enough to resist the shear force regardless of stirrup yield strength due to the concrete contribution to shear resistance. For G50 beams, when stirrup spacing decreased from 300 mm to 175 mm, failure mode shifted from stirrup-yielding control to concrete crushing control. Thus, the effect of stirrup with a spacing smaller than 175 mm is negligible. Moreover, several specimens did not exhibit extensive stirrup yielding at the peak load, indicating that the shear failure remained governed by diagonal compression or mixed shear-compression mechanisms rather than by yielding of transverse reinforcement alone.

5. Shear strength model

5.1. Application of existing design methods

Due to the inherent complexity of shear behavior, unlike flexural behavior, there is no international unified method for estimating the shear strength of reinforced and/or prestressed concrete members. To evaluate the applicability of current design codes in predicting the shear capacity of prestressed and non-prestressed GPC beams, a comparative study was conducted using GB50010–2010 [30], ACI 318–25 [31], AASHTO 2024 [32], CEB-FIP 2010 [33], Eurocode 2 [37], and JGC 15 [38]. The detailed shear strength prediction models adopted by these codes are summarized in Table 7. A total of 390 experimental data points [7,11–13,25,50–89] were collected for evaluation, including 266 prestressed PCC beams [7,50–82], 109 non-prestressed GPC beams [11–13, 25,83–89], and 15 prestressed GPC beams of this study. All data can be found in the supplementary materials.

GB 50010–2010 [30] directly incorporates the contribution of prestressing to shear strength, where the prestressing effect is represented by a term equal to 0.05 N_{p0}. ACI 318–25 [31] distinguishes between flexure-shear cracking resistance and web-shear cracking resistance in shear design prestressed members. However, the contribution of prestressing is considered only when the effective prestressing stress satisfies $f_{se} \geq 0.4\, f_{pu}$, and the prestressing effect is incorporated into the concrete shear resistance V_c. In both AASHTO-2024 [32] and Eurocode 2 [37], the contribution of prestressing is also incorporated into V_c. In contrast, JGC-15 [38] considers the effect of prestressing on the shear capacity through the ratio M_o/M_u, thereby indirectly accounting for the influence of prestressing.

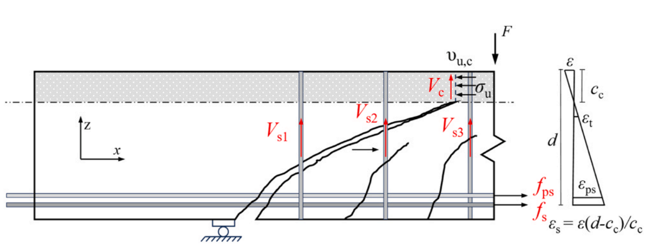

Fig. 15. Shear force mechanism of beams with stirrups.

For direct comparison, the measured of the materials were used instead of the design strengths specified in design codes, and all safety factors were set to 1.0. Fig. 14 compares the ratios of test results to predictions of shear capacities for six current design codes in accordance with key design parameters including concrete axial compressive strength (f'_c), shear span-to-depth ratio (λ), longitudinal reinforcement ratio (ρ_l), and shear reinforcement index ($\rho_v f_v$). The comparison indicates that the average predicted values (mean) of all codes except AASHTO 2024 are greater than 1, which means these design codes provide generally conservative predictions of shear capacity, thereby validating the applicability and safety margins of current design codes for GPC structural design. Furthermore, for specimens with lower stirrup ratios, the predictions were even more conservative, which would be attributed to an underestimation of the concrete contribution to the overall.

Among the six design codes, the predictions of AASHTO 2024 [32] agreed well with the experimental results, with a mean value of 0.996 and the smallest coefficient of variation (COV = 0.273), demonstrating superior accuracy and consistency. However, its predictions tend to be slightly unconservative in certain cases. ACI 318–25 [31] provided conservative predictions most of the beams (Mean = 1.277) and exhibited higher accuracy than other design codes for this category. The predictions of other codes are relatively conservative, with the ratio of experimental shear capacity to predicted shear capacity (V_{exp}/V_{pred}) being greater than 1. A general trend is that the prediction conservatism of all codes decreases with the increase in the shear-span ratio (λ) and stirrups reinforcement ($\rho_v f_v$). The main reason for the generally conservative predictions is that current codes underestimate the shear contribution of concrete for safety purposes, and do not account for the contribution of longitudinal reinforcement to shear resistance. For prestressed beams with low shear-span ratios, the arch action dominates the shear transfer mechanism, which is not fully considered in the existing code models, leading to notable underestimation of the shear capacity. However, the existing codes achieve only moderate prediction performance for non-prestressed GPC beams, and the distribution pattern of their test data points is similar to that of prestressed PCC beams. Besides, GB 50010–2010 [30] and ACI 318–25 [31] exhibited higher accuracy in predicting the strength of prestressed GPC beams of this study. For the experimental results obtained in the present study, both ACI 318–25 [31] and AASHTO 2024 [32] achieved satisfactory predictive accuracy, with the ratios V_{exp}/V_{pred} remaining close to unity.

5.2. Proposed shear strength model

In general, concrete beams exhibit two primary failure modes under shear force, namely early shear failure and flexural yielding-shear failure. The first mode is characterized by the rapid propagation of diagonal shear cracks that immediately penetrate the entire beam cross-section, leading to sudden failure at the peak load. This failure mode typically occurs in beams without stirrups or with insufficient shear reinforcement. The second mode occurs when an adequate amount of stirrups is provided. In this case, diagonal shear cracks develop but do not fully penetrate the concrete cross-section. As the applied load increases, the stirrups gradually reach their yield strength, followed by shear failure of the beam. Park et al. [9] proposed a method for predicting the shear strength of beams under flexure-shear failure based on the Rankine criterion, which has been shown to provide reasonably accurate predictions. However, the original Park model requires iterative calculations to determine the depth of the compressive zone and the concrete strain, resulting in high computational complexity and limited practicality for engineering applications. To overcome this limitation, the present study optimizes the calculation procedure of Park's model by simplifying the solution process into a direct analytical form. The accuracy of the simplified model is verified using the collected experimental data.

When excessive shear reinforcement is provided, the shear capacity

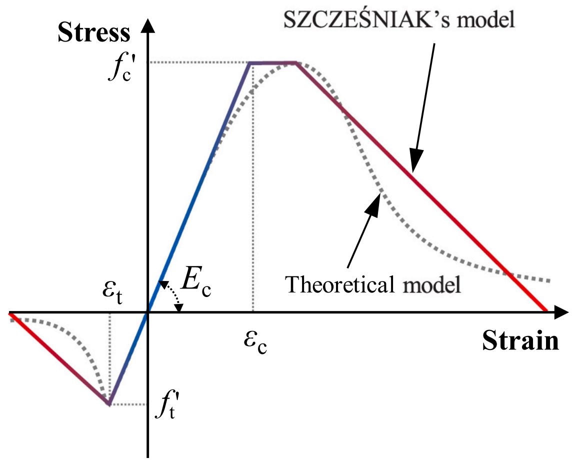

Fig. 16. Simplified concrete constitutive model [90].

of the beam exceeds concrete shear capacity, resulting in concrete crushing in the compression zone at the top of the beam. In this case, beams are governed by flexural failure. For the first failure mode (when $V_c > V_s$), the load-carrying capacity of the beam is governed primarily by concrete strength. In contrast, for the second failure mode, the load resistance depends on the composite action of concrete and reinforcement within the shear-critical region (Fig. 15). The shear strength of beam with stirrups can be defined as follows:

$$V = V_c + V_s \tag{1}$$

According to the Rankine criterion [36], the stress state of compressive strength failure is defined as follows:

$$\sigma_1 = -\frac{\sigma_u}{2} - \sqrt{\left(\frac{\sigma_u}{2}\right)^2 + v_{uc}^2} = -f'_c \tag{2}$$

In the tensile region of the uncracked zone, the relationship between the normal stress and shear stress can be defined as follows:

$$\sigma_2 = -\frac{\sigma_u}{2} + \sqrt{\left(\frac{\sigma_u}{2}\right)^2 + v_{ut}^2} = f'_t \tag{3}$$

where σ_1 and σ_2 are the principal compressive and tensile stresses, respectively; and σ_u are the compressive normal stress; and ν_{uc} and ν_{ut} are the shear stress at compression and tension region, respectively.

Due to the influence of compressive stress, the tensile strength f'_t under a combined stress state is lower than the uniaxial tensile strength f_t. For beams that fail in shear, the magnitude of the principal compressive stress is relatively small. Thus, for simplicity, the tensile strength under the combined stress state may be taken as $f'_t = f_t$. The relationship between the shear stress and principal stress (σ_u)of the sections governed by tensile (ν_{ut}) failure and compressive failure (ν_{uc}) can be expressed as follows:

$$v_{ut} = \sqrt{f'_t \cdot [f'_t + \sigma_u(\varepsilon)]} \tag{4}$$

$$v_{uc} = \sqrt{f'_c \cdot [f'_c - \sigma_u(\varepsilon)]} \tag{5}$$

The shear failure of beams is mainly dominated by **Eq. (4)**. Since calculation of shear capacity requires integration of **Eq. (4)**, the concrete constitutive model was simplified into a multilinear model $\sigma_u(\varepsilon) = f'_c\varepsilon/\varepsilon_0$, treating concrete as a linear elastic material following the methodology with Szcześniak [90] It should be noted that when the compressive strain of concrete exceeds (0.002 for PCC and 0.003 for GPC in general), the shear capacity is lost, and the shear force becomes zero.

The experimental results clearly indicate that the shear capacity of beams is affected by the longitudinal reinforcement ratio. An increase in the longitudinal reinforcement ratio enhances the compressive normal stress and concrete compression zone depth, thereby improving the shear capacity. The longitudinal reinforcement ratio should be taken into account to calculate the shear strength. During the calculation, the beam section is assumed to satisfy the plane section assumption. The force provided by the uncracked tension zone of the concrete is negligible. Based on the equilibrium of forces, the following relationship can be established:

$$b\int_0^{c_c} \sigma_{uc}(x,z)dz + \varepsilon_s' E_s' A_s' = \varepsilon_s E_s A_s + \varepsilon_{ps} E_{ps} A_{ps} \tag{6}$$

where ε_s, E_s, and A_s refer to the strain, elastic modulus, and area of the steel reinforcement in the tension zone, respectively; and ε_s', E_s', and A_s' correspond to the reinforcement in the compression zone. Similarly, the strain, elastic modulus, and area of the prestressing steel are represented by ε_{ps}, E_{ps}, and A_{ps}, respectively.

The compression zone depth is obtained as follows:

$$c_c = \frac{-B + \sqrt{B^2 - 4AC}}{2A} \tag{7}$$

where $A = bf_c'/(2\varepsilon_0)$, $B = E_s'A_s' + E_sA_s + E_{ps}A_{ps}$, $C = -(a_cE_s'A_s' + dE_sA_s + d_{ps}E_{ps}A_{ps})$. a_c and d_{ps} are the concrete cover in respect to compressive reinforcement and the beam depth in respect to strand, respectively.

However, during the actual loading process, as the shear span-to-depth ratio increases, the failure mode of the beam gradually shifts from shear failure to flexural failure. This transition leads to an increase in the crack height at the bottom of the section. Consequently, the compression zone depth (c) should be adjusted via regression analysis. Based on the collected experimental data, the modified compression zone depth is defined as follows:

$$c_{c,\lambda} = c_c/(\lambda - 0.6) \tag{8}$$

Adamu et al. [40] suggested that the ratio of the tensile concrete height within the cracked zone is related to the shear span-to-depth ratio, as follows:

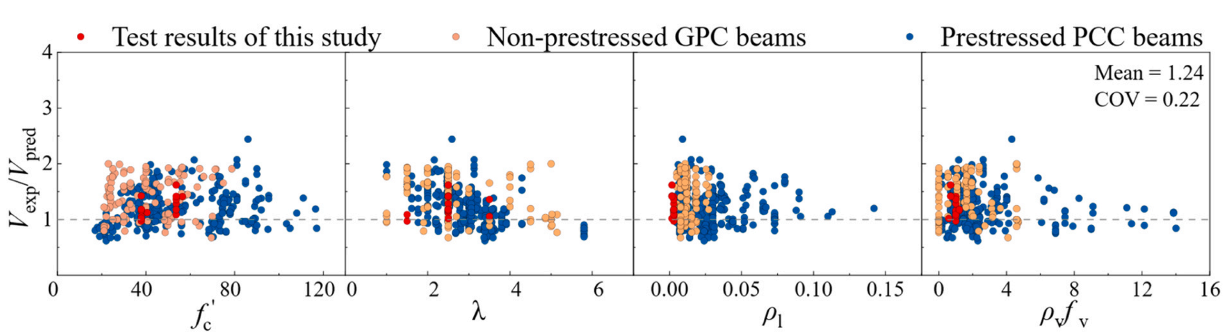

Fig. 17. Comparison of test results with predictions of the proposed model.

$$\alpha = \frac{c_t}{c_c + c_t} = 0.1(a/d)^{0.612} \tag{9}$$

The tensile strength of concrete is approximately 0.1 times its compressive strength [91]. Based on the linear assumption of the constitutive model adopted in this study, the cracking strain is taken as 0.1 times the peak compressive strain. Consequently, the maximum strain in the compression zone becomes as follows:

$$\varepsilon = \frac{(1-\alpha)\varepsilon_c}{10\alpha} \tag{10}$$

By integrating **Eq. (4)** over the cross-section, the shear capacity provided by the concrete is obtained as follows:

$$V_c = b\int_0^{c_{c,\lambda}} v_{ut}(z)dz = \frac{2bc_{c,\lambda}\sqrt{f_t'}}{3E_c\varepsilon}\left[\left(f_t' + f_{pc} + E_c\varepsilon\right)^{\frac{3}{2}} - \left(f_t' + f_{pc}\right)^{\frac{3}{2}}\right] \tag{11}$$

$$V_s = A_s f_v d/s \tag{12}$$

In addition, the size factor of the members is also incorporated into the shear strength prediction for more accurate calculations, which can be expressed as follows:

$$V = \lambda_s(V_c + V_s) \tag{13}$$

where a λ_s is the size factor about shear span in meters proposed by Zararis and Papadakis [92].

Fig. 17 illustrates the predictive performance of the newly proposed model. The proposed model provides relatively accurate predictions for the shear capacity of prestressed PCC beams and the prestressed GPC beams tested, with potential limitations for specimens with extreme parameter combinations. Overall, the ratio of experimental to predicted shear strength (V_{exp}/V_{pred}) centers closely around the unity line with a mean value of 1.24, signifying a generally high level of predictive accuracy. Although a coefficient of variation (COV) of 0.22, the majority of the data points are well-contained within the 0.5–2.0 range. Compared with current design codes (Fig. 14), the proposed model reasonably considered the influence of reinforcement ratio on the shear capacity. The prediction trends for non-prestressed GPC beams are consistent with those for prestressed concrete, demonstrating that the proposed model is effective in predicting the shear capacity for PCC and GPC materials. Also, the proposed calculation method is simpler than that of the literature [9]. Conversely, the prestressed PCC beams display a broader distribution, suggesting inherent complexities in the shear behavior of traditional prestressed members that lead to relatively reduce stability in predictions. Notably, the experimental results of this study are in high alignment with the broader dataset, thereby validating the universality of the proposed model.

6. Conclusions

As an emerging sustainable construction material, geopolymer concrete was investigated in this study through shear tests on fifteen prestressed beams. The test parameters included concrete strength, shear span-to-depth ratio, stirrup spacing, stirrup yield strength, and longitudinal reinforcement ratio. In addition, an extensive experimental database was compiled to evaluate the shear design provisions of current design codes, and a new shear strength model was proposed. The main conclusions can be summarized as follows:

1. Prestressed GPC beams exhibited shear capacities comparable to the counterpart prestressed PCC beams (a 2.8% lower shear capacity for 50 MPa GPC and 5.6% higher for 70 MPa PCC). However, GPC beams showed 76.1%-128.2% larger mid-span deflection at peak load, 36.7%-63.3% lower diagonal cracking load, and 2.9–3.0 times wider diagonal cracks at ultimate state. No significant differences were observed in the failure modes between prestressed GPC and PCC beams.
2. When the concrete compressive strength increased from 50 MPa to 70 MPa at a shear span-to-depth ratio of 2.5, the shear capacity increased by 43.4%. Compared with specimens with a shear span-to-depth ratio of 1.5, the shear capacity of beams with shear span-to-depth ratios of 2.5 and 3.5 decreased by approximately 37.4–38.4% and 52.8–58.6%, respectively. For G50 concrete beams, increasing the stirrup ratio from 0.95% to 1.42% led to an 11% increase in shear capacity. Moreover, increasing the longitudinal reinforcement ratio significantly enhanced the cracking resistance of the concrete.
3. When the longitudinal reinforcement ratio increased from 0.7 to 1.2%, the concrete compression zone depth was enlarged, resulting in an approximately 40% increase in the shear capacity of the prestressed GPC beams. Increasing stirrup ratio enhanced the shear capacity of the specimens, but this effect was limited for the G70 specimens. In contrast, increasing stirrup yield strength alone had a limited effect on improving the shear capacity in the case of G70 concrete when the minimum stirrups ratio requirement was satisfied.
4. A total of 390 experimental data points, including the collected present test results and existing test results, were used to evaluate shear capacity models specified in current design codes. The prediction trends for the shear strength of non-prestressed GPC beams were consistent with those for prestressed PCC beams. Furthermore, the current design codes were also applicable to predicting the shear strength of prestressed GPC beams, but only ACI 318–25 (i.e., mean V_{exp}/V_{pred} =1.277, and COV=0.345) and AASHTO 2024 (i.e., mean V_{exp}/V_{pred} =0.996, and COV=0.273) provided relatively accurate predictions of shear strength.
5. Based on the Rankine failure criterion, a new shear capacity model for prestressed beams was derived. The proposed method used simplified constitutive concrete model explained the contribution of reinforcement ratio to shear resistance, and demonstrated the improved prediction accuracy (i.e., mean V_{exp}/V_{pred} =1.24, and COV=0.22) compared with existing design approaches.

A major limitation is the absence of repeated tests. Future work is suggested to include replicate specimens for statistical analysis and examine the effect of GPC material uniformity on the variability of brittle shear failure.

CRediT authorship contribution statement

Guoxu Zhao: Writing – original draft, Visualization, Validation, Software, Methodology, Investigation, Formal analysis, Data curation. **Gao Ma:** Writing – review & editing, Supervision, Methodology, Investigation, Funding acquisition, Conceptualization, Validation, Project administration. **Hyeon-Jong Hwang:** Writing – review & editing, Investigation, Funding acquisition. **Caijun Shi:** Supervision, Funding acquisition. **Yunxing Du:** Validation, Conceptualization.

Declaration of Competing Interest

The authors declare that they have no known competing financial interests or personal relationship that could have appeared to influence the work reported in this paper.

Acknowledgements

This research was sponsored by the National Natural Science Foundation of China (Grant No. 51638008), the Huxiang Youth Talent Support Program of Hunan Province, China (Grant No. 2021RC3041), and the National Research Foundation of Korea (NRF) grant funded by the Korea government (MSIT) (Grant No. RS-2024–00409719).

Appendix A. Supporting information

Supplementary data associated with this article can be found in the online version at doi:10.1016/j.engstruct.2026.122874.

Data availability

Data will be made available on request.

References

[1] Davidovits J. Geopolymers: inorganic polymeric new materials. J Therm Anal Calorim 1991;37:1633–56.
[2] Duxson P, Provis JL, Lukey GC, Van Deventer JSJ. The role of inorganic polymer technology in the development of 'green concrete. Cem Concr Res 2007;37:1590–7.
[3] Bakharev T, Sanjayan JG, Cheng YB. Sulfate attack on alkali-activated slag concrete. Cem Concr Res 2002;32:211–6.
[4] Zhang HY, Kodur V, Wu B, Cao L, Wang F. Thermal behavior and mechanical properties of geopolymer mortar after exposure to elevated temperatures. Constr Build Mater 2016;109:17–24.
[5] Hassan A, Arif M, Shariq M. Use of geopolymer concrete for a cleaner and sustainable environment–A review of mechanical properties and microstructure. J Clean Prod 2019;223:704–28.
[6] Zwoyer EM, Siess CP. Ultimate strength in shear of simply-supported prestressed concrete beams without web reinforcement. ACI J. Proc. 1954;51:181–200.
[7] Elzanaty AH, Nilson AH. Shear capacity of prestressed concrete beams using high-strength concrete. ACI J. Proc. 1986;83:359–68.
[8] Rupf M, Ruiz MF, Muttoni A. Post-tensioned girders with low amounts of shear reinforcement: shear strength and influence of flanges. Eng Struct 2013;56:357–71.
[9] Park H-G, Kang S, Choi K-K. Analytical model for shear strength of ordinary and prestressed concrete beams. Eng Struct 2013;46:94–103.
[10] Albidah AS. Shear behviour of metakaolin-fly ash based geopolymer concrete deep beams. Eng Struct 2023;275:115271.
[11] Shibayama A, Nishiyama M. Shear strength of reinforced fly-ash-based geopolymer concrete beams with and without shear reinforcement. Structures 2023;50:603–14.
[12] Tauqir M, Qazi AU, Khan QS, Munir MJ, Kazmi SMS. Shear behavior of geopolymer concrete slender beams. Buildings 2023;13.
[13] Liu J, Yang H, Wang Y, Zhang G. Experimental and numerical study of shear bearing capacity of geopolymer concrete beams with stirrup. Int J Struct Integr 2025;16:1557–98.
[14] Mao Y, Song J, Hwang H-J, Du Y, Shi C. Shear behavior of reinforced slag-based geopolymer concrete T-shaped beams. Structures 2025;74:108491.
[15] Fathi ME, El-Zoughiby ME, Mortagi M, Youssf O, Abdulazeez M, Tahwia AM. Shear performance of sustainable self-compacting geopolymer RC beams: experimental and numerical study. Infrastructures 2026;11:84.
[16] Neupane K, Hadigheh SA. Sodium hydroxide-free geopolymer binder for prestressed concrete applications. Constr Build Mater 2021;293:123397.
[17] Neupane K, Hadigheh SA, Dias-da-Costa D. Numerical study on the structural behaviour of a geopolymer prestressed concrete beam. IOP Conference Series Materials Science Engineering 2019:311–7.
[18] Sonal T, Urmil D, Darshan B. Behaviour of ambient cured prestressed and non-prestressed geopolymer concrete beams. Case Stud Constr Mater 2022;16:e00798.
[19] Chu L, Tang Q, Feng H, Shi C, Du Y, Ding D, et al. Flexural performance of post-tensioned unbonded prestressed geopolymer concrete beams. Structures 2026;83:110906.
[20] Li T, Ma G, Navarro-Gregori J, Martí-Vargas JR, Shi C. Development length of prestressing strands in pretensioned geopolymer concrete beams. Eng Struct 2026;353:122344.
[21] Thumrongvut J, Seangatith S, Phetchuay C, Suksiripattanapong C. Comparative experimental study of sustainable reinforced Portland cement concrete and geopolymer concrete beams using rice husk ash. Sustainability 2022;14:9856.
[22] Visintin P, Ali MSM, Albitar M, Lucas W. Shear behaviour of geopolymer concrete beams without stirrups. Constr Build Mater 2017;148:10–21.
[23] Huang Z, Chen W, Hao H, Chen Z, Pham TM, Tran TT, et al. Shear behaviour of ambient cured geopolymer concrete beams reinforced with BFRP bars under static and impact loads. Eng Struct 2021;231:111730.
[24] Zhang HY, Yan J, Kodur V, Cao L. Mechanical behavior of concrete beams shear strengthened with textile reinforced geopolymer mortar. Eng Struct 2019;196:109348.
[25] Wu C, Hwang H-J, Shi C, Li N, Du Y. Shear tests on reinforced slag-based geopolymer concrete beams with transverse reinforcement. Eng Struct 2020;219:110966.
[26] Madheswaran CK, Ambily PS, Lakshmanan N, Dattatreya JK, Sathik SAJ. Shear behavior of reinforced geopolymer concrete thin-webbed t-beams. Acids Mater J 2014;111:89.
[27] Building Code Requirements for Structural Concrete (ACI 318–08) and Commentary. Farmington Hills, MI: Institute AC..
[28] Aldemir A, Akduman S, Kocaer O, Aktepe R, Sahmaran M, Yildirim G, et al. Shear behaviour of reinforced construction and demolition waste-based geopolymer concrete beams. J Build Eng 2022;47:103861.
[29] Irmawaty R, Ekaputri JJ. Experimental and analytical study for shear strengthening of reinforced-concrete beams using a prefabricated geopolymer–mortar panel. Case Stud Constr Mater 2022;17:e01568.
[30] GB50010–2010, Code for design of concrete structures. Beijing, China: Ministry of Housing and Urban-Rural Development of China..
[31] ACI Committee 318. Building Code Requirements for Structural Concrete and Commentary (ACI 318–25). Farmington Hills, MI, USA: American Concrete Institute..
[32] AASHTO, LRFD Bridge Design Specifications, 10th Edition. Washington, D. C.: American Association of State Highway and Transportation Officials..
[33] Model Code 2010-Final Draft: Volume 2.: Walraven JC..
[34] Choi K-K, Hong-Gun P, Wight JK. Unified shear strength model for reinforced concrete beams-Part I: development. Acids Struct J 2007;104:142.
[35] Choi K-K, Hong-Gun P. Unified shear strength model for reinforced concrete beams-Part II: verification and simplified method. Acids Mater J 2007;104:153.
[36] Rankine WJM. On the stability of loose earth. Proc R Soc Lond 1856:185–7.
[37] Eurocode 2: Design of concrete structures – Part 1–1: General Rules and Rules for Buildings,.: European Committee for Standardization..
[38] Standard Specifications for Concrete Structures-2007 "Design". Tokyo, Japan: Concrete Committee of Japan Society of Civil Engineers..
[39] Dinh NH, Nguyen CV, Bui QH. Mechanical model for shear strength prediction of corrosion-damaged reinforced concrete beams under various corrosion schemes. Eng Struct 2025;335:120357.
[40] Adamu SN, Aure TW, Mohammed TA, Hantouche EG. An advanced prediction model for shear strength of slender reinforced concrete beams: integrating shear transfer mechanisms and size effects. Struct Concr 2025.
[41] Standard for test methods of concrete physical and mechanical properties(GB/T 50081–2019). Beijing: China MoCotPsRo. Ministry of Construction of the People's Republic of China.
[42] Liu Y, Hwang H-J, Mao Y, Du Y, Su J, Hu X, et al. Bond performance of steel rebar in alkali-activated slag-based concrete after exposure to elevated temperature. Constr Build Mater 2023;394:132281.
[43] Du Y, Wang J, Shi C, Hwang H-J, Li N. Flexural behavior of alkali-activated slag-based concrete beams. Eng Struct 2021;229:111644.
[44] Standard for test methods of concrete structures (GB/T 50152–2012). Beijing: China. MoHaU-RDotPsRo. Ministry of Housing and Urban-Rural Development of the People's Republic of China..
[45] GB/T 28900. Test methods of steel for reinforcement of concrete. Beijing: China Iron & Steel Association.
[46] GB/T 21839. Steel for Prestressed Concrete-Test Methods. Beijing: China Iron & Steel Association.
[47] Dai L, Tao Y, Yuan P, Wang L. 3D meso-scale modeling of bond behavior between helical strand and concrete. Eng Struct 2024;309:118041.
[48] Hutagi A, Khadiranaikar RB. Flexural behavior of reinforced geopolymer concrete beams. 2016 International Conference on Electrical. In: Electronics, and Optimization Techniques. IEEE; 2016. p. 3463–7.
[49] Nath P, Sarker PK. Flexural strength and elastic modulus of ambient-cured blended low-calcium fly ash geopolymer concrete. Constr Build Mater 2017;130:22–31.
[50] Villamizar S, Ramirez JA, Aguilar G. Shear strength and behavior of high-strength concrete prestressed beams. Acids Struct J 2017;114.
[51] Tawfiq KS. Cracking and shear capacity of high strength concrete girders. Tallahassee, FL: Final Report. FAMU/FSU College of Engineering; 1995.
[52] Shahawy MA, de V, Batchelor B. Shear behavior of full-scale prestressed concrete girders: comparison between AASHTO specifications and LRFD code. PCI J 1996;41.
[53] Mattock AH, Kaar PH. Precast-prestressed concrete bridges: 4. Shear tests of continuous girders. Concrete Bridges; 1961.
[54] Xuan XY. Effectiveness of welded wire fabric as shear reinforcement in pretensioned prestressed concrete T-beams. ACI Struct. J. 1988;85:429–36.
[55] Sato T, Ishibashi T, Yamashita Y, Takada. Shear strength and failure mode of prestressed concrete beams. Trans Jpn Concr Inst 1987;9:323–8.
[56] Robertson IN. Shear Strength of Prestressed Concrete T-Beams With Welded Wire Fabric as Shear Reinforcement. PCI J. 1987;32:46–61.
[57] Rangan BV. Web crushing strength of reinforced and prestressed concrete beams. Struct J 1991;88:12–6.
[58] Moayer M, Regan PE. Shear strength of prestressed and reinforced concrete T-beams. Spec Publ 1974;42:183–214.
[59] Maruyama K, Rizkalla SH. Shear design consideration for pretensioned prestressed beams. Struct J 1988;85:492–8.
[60] Lyngberg BS. Ultimate shear resistance of partially prestressed reinforced concrete I-beams. ACI J. Proc. 1976;73:214–22.
[61] Lee S-C, Cho J-Y, Oh B-H. Shear behavior of large-scale post-tensioned girders with small shear span-depth ratio. Acids Struct J 2010;107.
[62] Laskar A, Hsu TTC, Mo YL. Shear strengths of prestressed concrete beams part 1: experiments and shear design equations. Acids Struct J 2010;107.
[63] Labonte T., Hamilton Iii H.R. Self-consolidating concrete (SCC) structural investigation. 2005.
[64] Labib EL, Dhonde HB, Hsu TTC, Mo YL. Shear design of high strength concrete prestressed girders. Front Struct Civ Eng 2014;8:373–87.
[65] Kaufman MK, Ramirez JA. Re-evaluation of the ultimate shear behavior of high-strength concrete prestressed I-beams. Struct J 1988;85:295–303.
[66] Kang GY, Wu ZM, Wang LY, Xue BH. Ultimate shear tests of prestressed concrete I-beams. Proceedings of the Institution of Civil Engineers, 87; 1989. p. 401–14.
[67] Imano HIK, Kishi N, Kakemoto S. Loading tests of large prestressed reinforced concrete beams with different shear safety margin. Trans Jpn Concr Inst 2001;23:631–6.
[68] Hovell C, Avendaño A, Dunkman D, Moore A, Bayrak O, Jirsa J. Behavior of Texas U-beams and box-beams at prestress transfer and under shear loads. Austin: University of Texas; 2010.

[69] Hovell C, Avendaño A, Bayrak O, Jirsa J. Shear testing of prestressed concrete U-beams. Acids Struct J 2014;111:1253.
[70] Hernandez G. Strength of prestressed concrete beams with web reinforcement. SRS-153. Civ Eng Stud 1958.
[71] Heckmann C, Bayrak O. Effects of increasing the allowable compressive stress at release on the shear strength of prestressed concrete girders. Tex Dep Transp Res Technol Implement 2008.
[72] Hartman DL, Breen JE, Kreger ME. Shear Capacit High Strength Prestress Concr girders 1988.
[73] Hanson JM, Hulsbos CL. Ultimate shear tests of prestressed concrete i-beams under concentrated and uniform loadings. PCI J 1964;9:15–28.
[74] Garber DB, Gallardo JM, Deschenes DJ, Bayrak O. Nontraditional shear failures in bulb-t prestressed concrete bridge girders. J Bridge Eng 2016;21:04016030.
[75] De Wilder K, Lava P, Debruyne D, Wang Y, De Roeck G, Vandewalle L. Experimental investigation on the shear capacity of prestressed concrete beams using digital image correlation. Eng Struct 2015;82:82–92.
[76] De Silva S., Witchukreangkrai E. Experimental study on shear cracking behavior in I-shaped partially prestressed concrete beams. コンクリート工学年次論文集= Proceedings of the Japan Concrete Institute/日本コンクリート工学協会 編. 2006; 28:817-822.
[77] Choulli Y, Marí AR, Cladera A. Shear behaviour of full-scale prestressed i-beams made with self compacting concrete. Mater Struct 2008;41:131–41.
[78] Bruce Jr RN. An experimental study of the action of web reinforcement in prestressed concrete beams. Univ Ill Urbana-Champaign 1962.
[79] Bennett EW, Debaiky SY. High strength steel as shear reinforcement in prestressed concrete beams. Spec Publ 1974;42:231–48.
[80] Bennett EW, Balasooriya BMA. Shear Strength Prestress beams thin webs Fail Inclin Compress 1971:204–12.
[81] Avendaño A.R., Bayrak O. Shear strength and behavior of prestressed concrete beams. Technical Rep IAC-88-5DD1A003. 2008;3.
[82] Alshegeir A, Ramirez JA. Strut-tie approach in pretensioned beams. Struct J 1992; 89:296–304.
[83] Visintin P, Mohamed Ali MS, Albitar M, Lucas W. Shear behaviour of geopolymer concrete beams without stirrups. Constr Build Mater 2017;148:10–21.
[84] Ozturk M, Arslan G. Shear behavior of granulated blast furnace slag-based geopolymer-reinforced concrete beams. Buildings 2022;12.
[85] Lee K-M, Choi S, Choo JF, Choi Y-C, Yoo S-W. Flexural and shear behaviors of reinforced alkali-activated slag concrete beams. Adv Mater Sci Eng 2017;2017: 1–12.
[86] Darmawan MS, Bayuaji R, Sugihardjo H, Husin NA, Anugraha Affandhie RB. Shear strength of geopolymer concrete beams using high calcium content fly ash in a marine environment. Buildings 2019;9.
[87] Albidah AS. Shear behviour of metakaolin-fly ash based geopolymer concrete deep beams. Eng Struct 2023;275.
[88] Madheswaran CK, Ambily PS, J K, Dattatreya NL. Shear behavior of reinforced geopolymer concrete thin-webbed T-beams. Acids Mater J 2014;111:89–97.
[89] Song J. Experimental research on shear performance of geopolymerconcrete T-beams [Master]. Hunan University; 2023 (In Chinese).
[90] Szcześniak A, Stolarski A. A simplified model of concrete for analysis of reinforced concrete elements. Mil. Technol. Sci. 2016;65:55–68.
[91] Lee J, Fenves GL. Plastic-damage model for cyclic loading of concrete structures. J Eng Mech 1998;124:892–900.
[92] Zararis PD, Papadakis GC. Diagonal shear failure and size effect in RC beams without web reinforcement. J Struct Eng 2001;127:733–42.